FPRINT-93-10

16 December 1992

Aspects of the SDSS Filter Complement

J. Smetanka
R. Kron

NO AFF

FPRINT-93-10

Abstract

This report gives preliminary results of testing the behavior of certain combinations of filters with respect to sometimes realistic spectral energy distributions for galaxies (in the context of deriving photometric redshifts), quasars at very high redshifts, and very cool dwarf stars. The purpose of this report is to generate ideas for what steps to take next.

Filters

The filters u,g,r,i are adopted from the Blue Book. The only change has been to the absolute sensitivity of the u filter; we have adopted twice the sensitivity given in the Blue Book. (Since Table 4.1c gives the count rate and S/N for the combination of two "old" u-band CCDs, that table still applies for a single new u-band, neglecting the effect of read noise.)

We have concocted a "z" filter with effective wavelength of about 9000 Å according to a recipe supplied by Jim Gunn and Don Schneider. In addition, we have invented another band called g* that is nested within the existing g band; it occupies the blueward half of the g-band's sensitivity function, and the peak sensitivity is set equal to the peak sensitivity of the original g band (Figure 1).

The effect of absorption in the Earth's atmosphere has been included in the filter transmission functions (the absorption as a function of wavelength was provided by Don Schneider).

The various filter complements with which we have experimented are as follows:

u g r i
u g r i z
u g* g r i
u u g r i.

Fermilab Library
0 1160 0021846 5

The last-named complement corresponds to having two CCDs with the same u band, as in the original plan, but now each has double the original sensitivity.

Noise Background

The only source of noise that we have considered is sky brightness. This is a reasonable presumption given enhanced sensitivity for the u band. The sky flux is the Turnrose (1974) Palomar night sky spectrum.

First-Order Check

Given the adopted sensitivities and noise, as a check we have reproduced the count rates and signal-to-noise ratios given in the Blue Book. All magnitudes quoted throughout this report are on the AB system. The values corresponding to Table 4.1c of the Blue Book for the filters given below.

```
# S/N as a function of AB magnitude for used in the SDSS simulation
# u g r i bands from blue book.  z band calculated in same manner.
# Simulations with 2 u band CCDs have S/N(2u) = 1.414*S/N(u)
# Simulations with the gstar filter have S/N(gstar) = 0.707*S/N(g)
# AB
# mag   u     g     r     i     z
#
 17.0 204.4 352.4 319.8 279.6 173.3
 17.5 160.7 277.4 250.1 212.6 129.5
 18.0 125.7 217.2 193.9 158.6  94.7
 18.5  97.5 168.8 148.6 115.7  67.4
 19.0  74.7 129.8 112.1  82.2  46.8
 19.5  56.4  98.3  82.8  56.9  31.7
 20.0  41.7  73.0  59.7  38.5  21.0
 20.5  30.0  52.9  41.9  25.5  13.7
 21.0  21.1  37.4  28.7  16.6   8.9
 21.5  14.5  25.7  19.2  10.7   5.7
 22.0   9.7  17.3  12.6   6.9   3.6
 22.5   6.4  11.4   8.2   4.4   2.3
 23.0   4.1   7.4   5.3   2.8   1.5
 23.5   2.7   4.8   3.4   1.8   0.9
 24.0   1.7   3.1   2.1   1.1   0.6
 24.5   1.1   1.9   1.4   0.7   0.4
 25.0   0.7   1.2   0.9   0.4   0.2
```

Photometric Redshifts for Galaxies

The goal is to explore the relative abilities of the various filter complements to distinguish between different redshifts on a galaxy-by-galaxy basis, given unknown intrinsic spectral energy distributions.

We have adopted model spectral energy distributions of Bruzual, specifically the $\mu = 0.5$ model from the most recent distribution (Galaxy Isochrone Synthesis Spectral Evolution Library, Bruzual and Charlot 1993). The energy distributions are specified at intervals of 2.5 Å to 20 Å in the rest frame, depending on the wavelength range. For convenience, we use the same model as seen at different ages to cover the range of intrinsic colors (this is unorthodox, but probably no worse a representation than many others!). We have selected a total of 27 ages or color types to span the range of possible spectral energy distributions, from 4.2×10^6 yr to 20×10^9 yr. Figure 2 shows selected examples of SED's from this set. We are currently working on incorporating emission lines into the model spectra, using our empirical relation between average line strength and rest-frame color.

Given these 27 SEDs, for each filter complement we can compute the corresponding colors as a function of redshift. We compute on a grid $z = 0.0$ to $z = 1.0$ in steps of $\Delta z = 0.01$. Figures 3, 4, 5, and 6 give various two-dimensional cuts through this color space. The boxes represent $z = 0$, and plus signs are spaced every $\Delta z = 0.2$.

Important types of systematic errors cannot be explored with this machinery, but we can look at the effect of random errors due to photon statistics. We choose a particular S/N in a particular band, corresponding to a given apparent magnitude, and then evaluate the errors in all the bands and in the colors. The following table gives the selected options for the magnitudes:

g = 21.5, S/N = 25
g = 22.5, S/N = 12.5
r = 21.2, S/N = 25
r = 22.0, S/N = 12.5.

These S/N values refer to point sources; real galaxy images will be worse. Plots are included only for the first one in order to keep this report short.

For each complement of 4 or 5 filters, there is a corresponding multidimensional color space within which we have the model grid consisting of the 27 SEDs and 101 redshift steps. For each of the chosen apparent magnitudes given above, for each grid point we can compute the size in color space of the one-sigma error box. We can then estimate the maximum range of nominal redshifts, Δz, that is spanned by the error box and hence generate, for each SED, a measure of the uncertainty in redshift as a function of redshift.

This procedure is conservative (i.e., yields an overestimate of the errors) on two grounds:

1) we consider the color errors taken separately rather than combined; the volume of the error box is larger than the volume of a realistic error ellipse. In other words, the range of redshifts Δz we compute is the "worst-case" range, rather than the probable range.

2) in practice, one will discover that certain regions of the multidimensional color space are better measured with certain linear combinations (weights) for the filters. It is likely that there are a very large number of plausible optimization schemes. To maintain some interpretability of the results, *we have not attempted any such scheme*. (It may be more sensible to optimize with real data anyway, rather than pursuing it with model spectral energy distributions.)

On the other hand, none of this tests for departures between these model energy distributions and real galaxy energy distributions. In practice, one will use spectroscopically measured redshifts and multiband photometry of the same objects to tweak the calibration of the model grid. Moreover, there will of course be finite cosmic scatter in colors for galaxies at any redshift.

In order to visualize the large amount of information generated by the computations, we have chosen to display the SED - redshift space as threshholded by the value of Δz. Plots are attached that show 25 SEDs (the two bluest are always awful, and are omitted from the plots) represented as horizontal lines, each plotted against redshift. The bluest galaxies are at the bottom of each plot, and the reddest galaxies are at the top. White space indicates that the redshift range Δz is larger than 0.2, small dots are plotted for $0.1 < \Delta z < 0.2$, and crosses are plotted for $\Delta z < 0.1$. (Note that we use Δz as opposed to $\Delta z/z$ because of the behavior at low z.) Each plot (Figures 7, 8, 9, and 10) is for a different filter complement, as indicated.

Note that the bluest galaxies are almost always poorly measured. This is because their SEDs are nearly flat and nearly featureless; hence no "key" is available to determine the redshift from broad-band information. In the plots not included here, for $S/N)_g = 12.5$ and for $S/N)_r = 25$ and 12.5, the reddest galaxies are often poorly measured, especially at high redshift, despite the fact that they have large curvature in their SEDs and so might be expected to be measured well. Such galaxies however have very poorly measured u magnitudes: the u-g color will then span a wide range of redshifts, and the algorithm naively selects the largest Δz. If the S/N in the u band is less than 3, the

galaxy is deemed to be "undetected," and the fit takes place in a lower-dimensional space, with the same qualitative result. The g-band limited samples look better than the r-band limited samples, despite the nominally similar S/N, because the r-band limited samples will have worse S/N in the u band. (It is also known that very red galaxies show a dispersion in their ultraviolet fluxes, which is not modelled by our grid of SEDs.) In practice one would apply proper weightings to avoid being sensitive to large errors in u.

High-Redshift Quasars

The spectra of quasars at high redshift are strongly modulated by line blanketing in the Lyman α forest. This makes them harder to detect in bluer bands, but makes them easier to recognize because of their peculiar (red) colors. We have undertaken some simple computations of the expected colors and signal-to-noise ratios for quasars in the interval $4.5 < z < 7$ in the r,i,z bands. These computations are very similar to ones Don Schneider has already shown.

The model spectral energy distributions are composed of three elements: a power-law continuum ($\alpha = -0.5$ and -0.9), emission lines (as used by Warren et al. 1991 and Giallongo and Trevese 1990), and Lyman α forest and Lyman continuum systems, as specified by the same authors. The blanketing shortward of Lyman α emission is an average over the quasar population, and is modelled as a smooth function of redshift. The model was checked against the more recent, direct determination of the D_A and D_B parameters of Schneider, Schmidt, and Gunn (1991). The model predicts somewhat milder blanketing than is observed, but it may be that the sample of high-redshift quasars of SSG is biased to higher blanketing by observational selection. In any event, the milder blanketing used here is conservative in the sense that quasars will have less extreme colors and may thus look less unlike stars.

The table below gives the magnitudes, statistical errors, and r-i and i-z colors for the model quasar as a function of redshift. In one case, the i magnitude is fixed at i = 21 and the absolute magnitude that corresponds to this is computed (Figure 11), and in the other case the absolute magnitude M(1450) is fixed at -26.0 and the apparent i magnitude is computed (Figure 12). In both cases we use $q_0 = 0.5$ and $h = 0.5$. The color trends depend very little on the spectral index α. Rather, the behavior at large redshift is dominated by the assumed extrapolation of the blanketing in the Lyman α forest; even the qualitative trends may not be realistic.

Simulated broad-band colors and magitudes for high redshift quasars. Quasar spectra are from TANK simuation code (12-92). Assumes M(1450) = M(7000) + 0.85. That is alpha = -0.5.
AB magnitudes:
(Ho=50 qo=0.5)

redshift	i M(1450)=-26	z	r-i	i-z	M(1450) i=21.0
4.0	19.73	19.69	0.02	0.03	-24.73
4.5	19.86	19.75	0.36	0.10	-24.86
5.0	19.99	19.95	1.63	0.03	-24.99
5.5	20.56	20.24	2.43	0.31	-25.56
6.0	21.20	20.31	2.31	0.88	-26.20
6.5	23.35	20.95	1.16	2.39	-28.35
7.0	23.79	21.86	2.79	1.92	-28.79

For alpha = -0.9, M(1450) = M(7000) + 1.54.

redshift	i M(1450)=-26	z	r-i	i-z	M(1450) i=21.0
4.0	19.74	19.64	0.12	0.09	-24.74
4.5	19.90	19.75	0.45	0.14	-24.90
5.0	20.08	19.98	1.70	0.09	-25.08
5.5	20.67	20.30	2.54	0.36	-25.67
6.0	21.32	20.41	2.43	0.90	-26.32
6.5	23.50	21.06	1.26	2.43	-28.50
7.0	24.02	21.99	2.81	2.02	-29.02

Very Cool Stars

The z filter option has also attracted attention because of its potential for identifying very cool dwarf stars or possibly brown dwarfs. We have accordingly modelled the r-i and i-z colors for various cool objects, first to determine the corresponding S/N, and second to explore how distinctive (say, with respect to high-redshift quasars) these colors are. So far we have not found a large body of spectrophotometry of cool stars that covers a large range of wavelength and is in convenient digital form. There do exist published plots for five low-luminosity stars in Henry and Kirkpatrick (1990) that cover the range 6320 - 9170 Å. In the meantime, we have simply used the scans of late-type dwarfs in the Gunn and Stryker (1983) atlas, and we have calculated the colors of low-temperature blackbodies as a

reference. The blackbody models actually fall surprisingly close to the M dwarfs (Figure 13).

Conclusions

There is a lot more work to be done concerning photometric redshift determination. We have made no attempt to determine optimum weighting schemes for the colors, and we are still evaluating the effect of emission lines. Also, we have not put any this gain onto a "science-per-dollar" basis. As expected, the z band separates quasars at $z > 6$ from the stellar locus as long as the i band flux is detected; however, this conclusion depends very strongly on the unknown behavior of the Lyman α forest at these redshifts. The expected low surface density of quasars at very high redshift means that to recognize them requires an evaluation of how many other objects may populate this region of color space (say, because of photometric errors).

A number of other issues related to the selection of a filter set warrant further study. These include but are not limited to secondary calibration of the spectroscopic survey using the broad-band fluxes, determination of reddening along a given line of sight, and recognition of low-metallicity stars.

Bruzual A., G. and Charlot, S. 1993 405, xx.
Giallongo, E. and Trevese, D. 1990, Ap.J. 353, 24.
Gunn, J.E. and Stryker, L. 1983 Ap. J Suppl., 52, 121.
Schneider, D.P., Schmidt, M. and Gunn, J.E. 1991 A.J., 101, 2004.
Turnrose, B.E. 1974 P.A.S.P., 86, 545.
Warren et al. 1991 Ap. J. Suppl. 76, 1.
Henry, T.J. and Kirkpatrick, J.D. 1990 Ap.J., 354, L29.

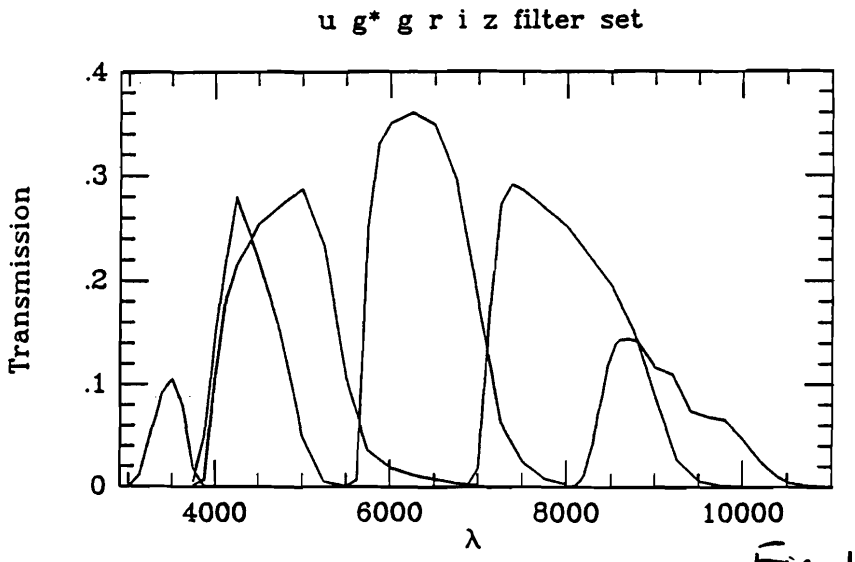
u g* g r i z filter set
Transmission
.4
.3
.2
.1
0
4000
6000
8000
10000
λ

Fig 1

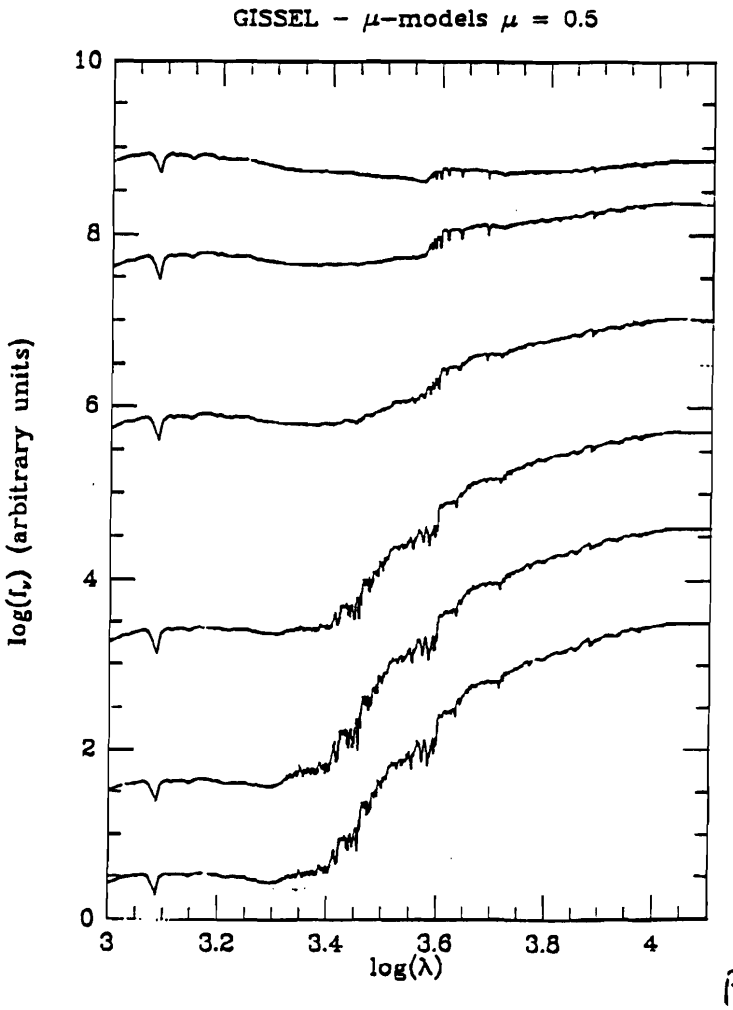
GISSEL – μ–models μ = 0.5
log(f_ν) (arbitrary units)
10
8
6
4
2
0
3
3.2
3.4
3.6
3.8
4
log(λ)

Fig 2

NOAO/IRAF V2.9.1EXPORT jtank@bucephalus.uchicago.edu Mon 19:47:32 14-Dec-92
mu.sub.ABmag.db
plus: redshift==0. || 0.195<redshift<0.205 || 0.395<redshift<0.405
plus: 0.595<redshift<0.605 || 0.795<redshift<0.805 || redshift==1.0
point: default

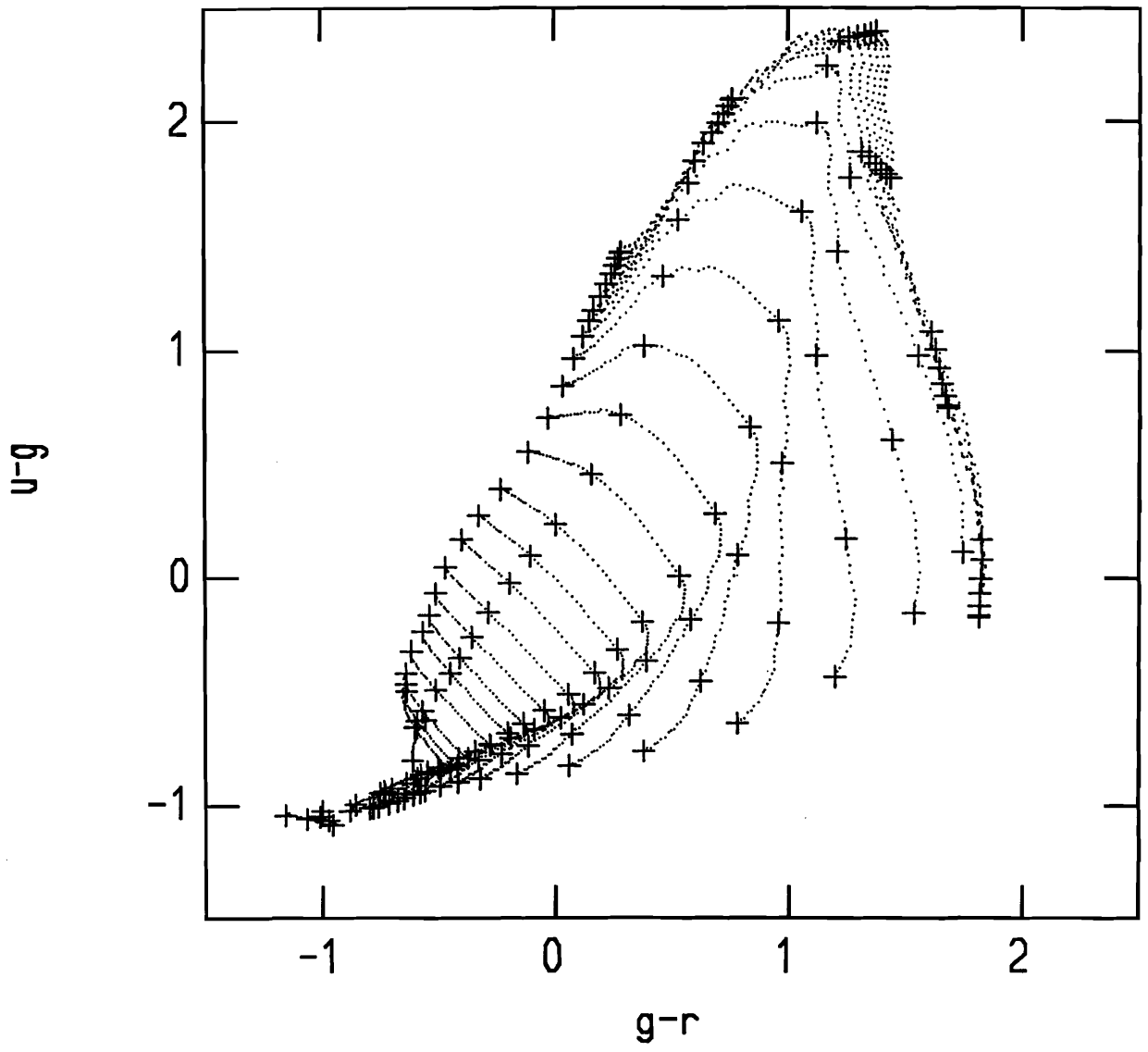

Fig 3

NOAO/IRAF V2.9.1EXPORT jtank@bucephalus.uchicago.edu Mon 19:48:06 14-Dec-92
mu.sub.ABmag.db
plus: redshift==0. || 0.195<redshift<0.205 || 0.395<redshift<0.405
plus: 0.595<redshift<0.605 || 0.795<redshift<0.805 || redshift==1.0
point: default

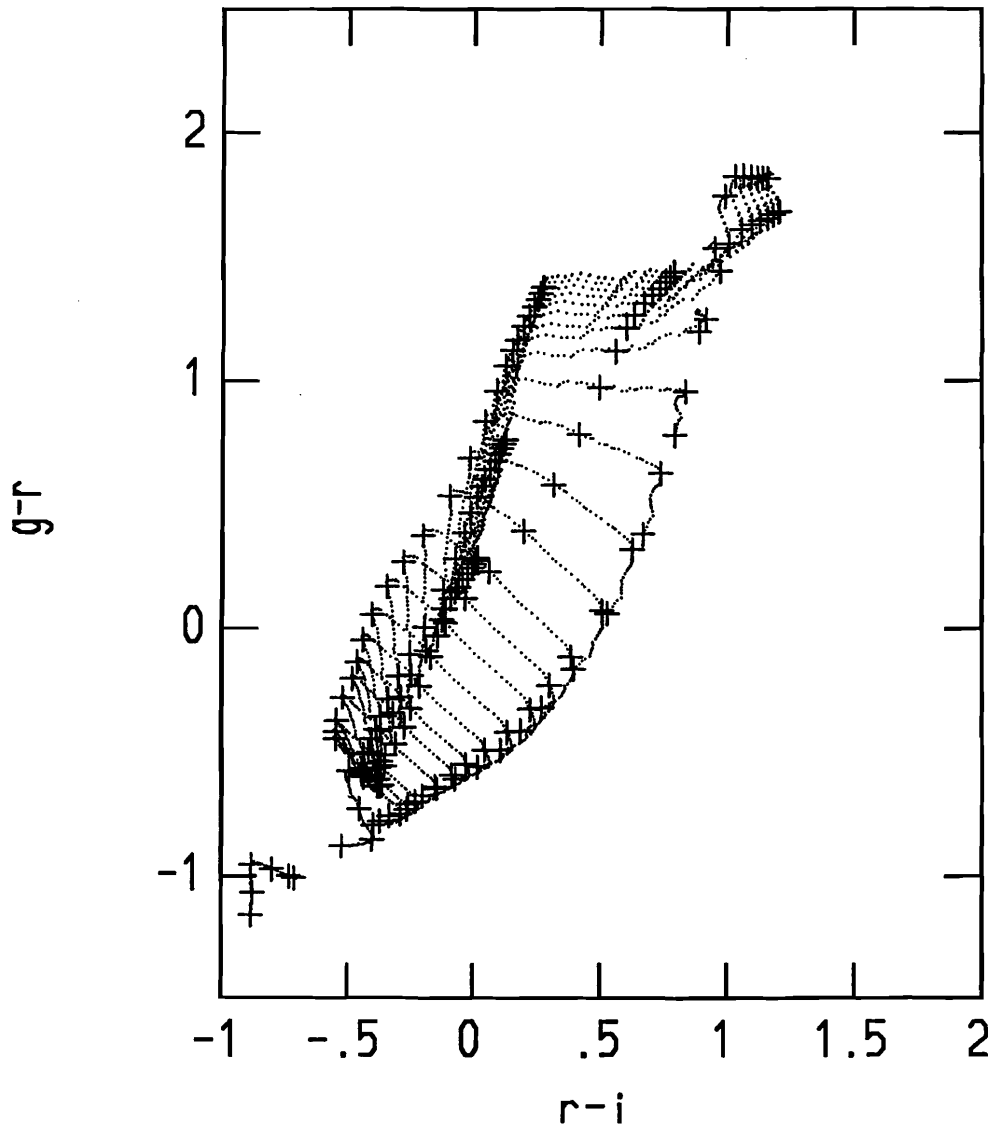

Fig 4

NOAO/IRAF V2.9.1EXPORT jtank@bucephalus.uchicago.edu Mon 19:48:32 14-Dec-92
mu.sub.ABmag.db
plus: redshift==0. || 0.195<redshift<0.205 || 0.395<redshift<0.405
plus: 0.595<redshift<0.605 || 0.795<redshift<0.805 || redshift==1.0
point: default

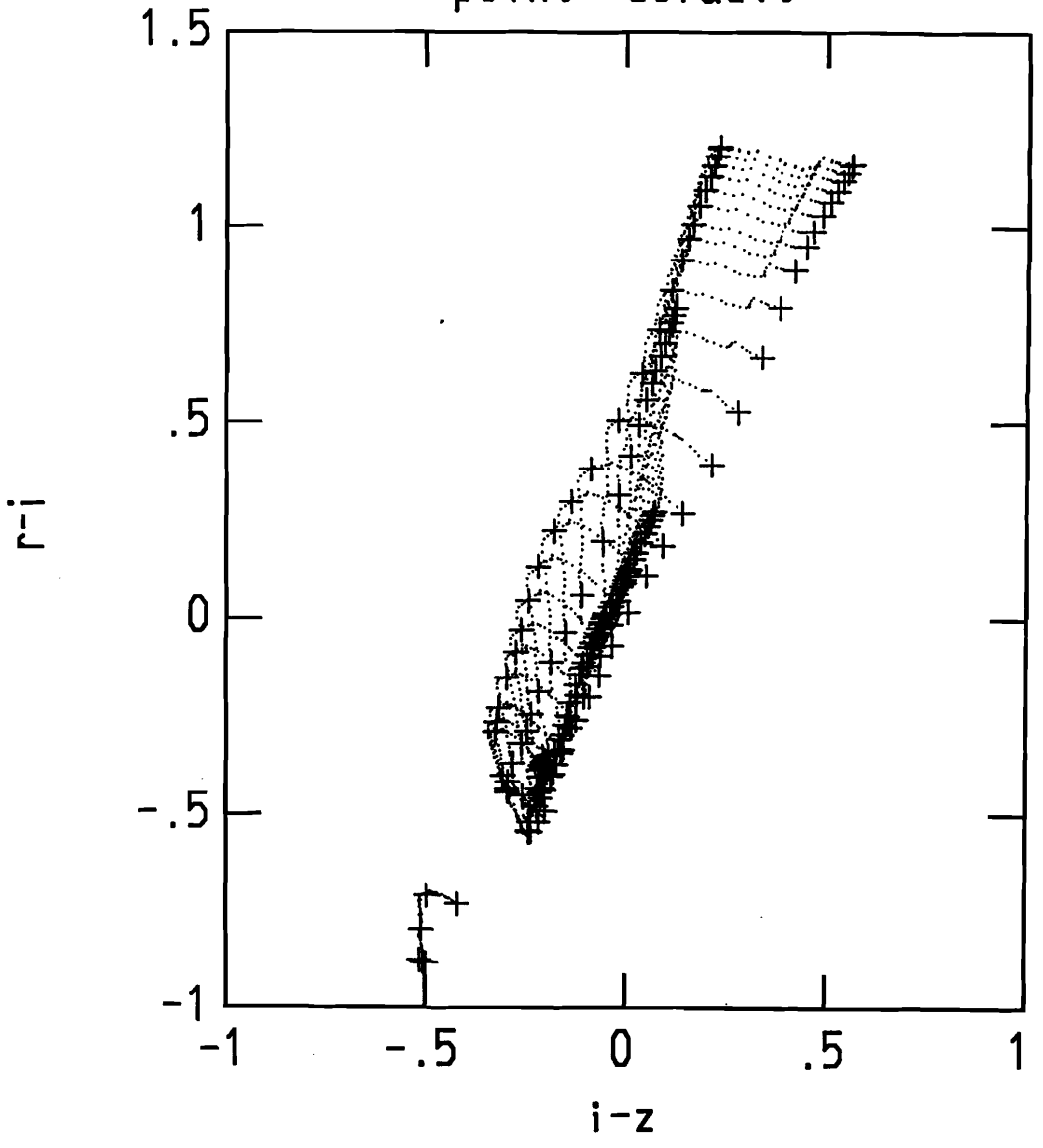

Fig 5

12-15-92 09:00EST FROM CHICAGO ASTROPHYSICS P23

NOAO/IRAF V2.10EXPORT jtank@oddjob.uchicago.edu Tue 16:55:28 15-Dec-92
mu.models.new.mag
plus: redshift==0 || 0.195<redshift<0.205
plus: 0.395<redshift<0.405 || 0.595<redshift<0.605
plus: 0.795<redshift<0.805 || redshift==1 point: default

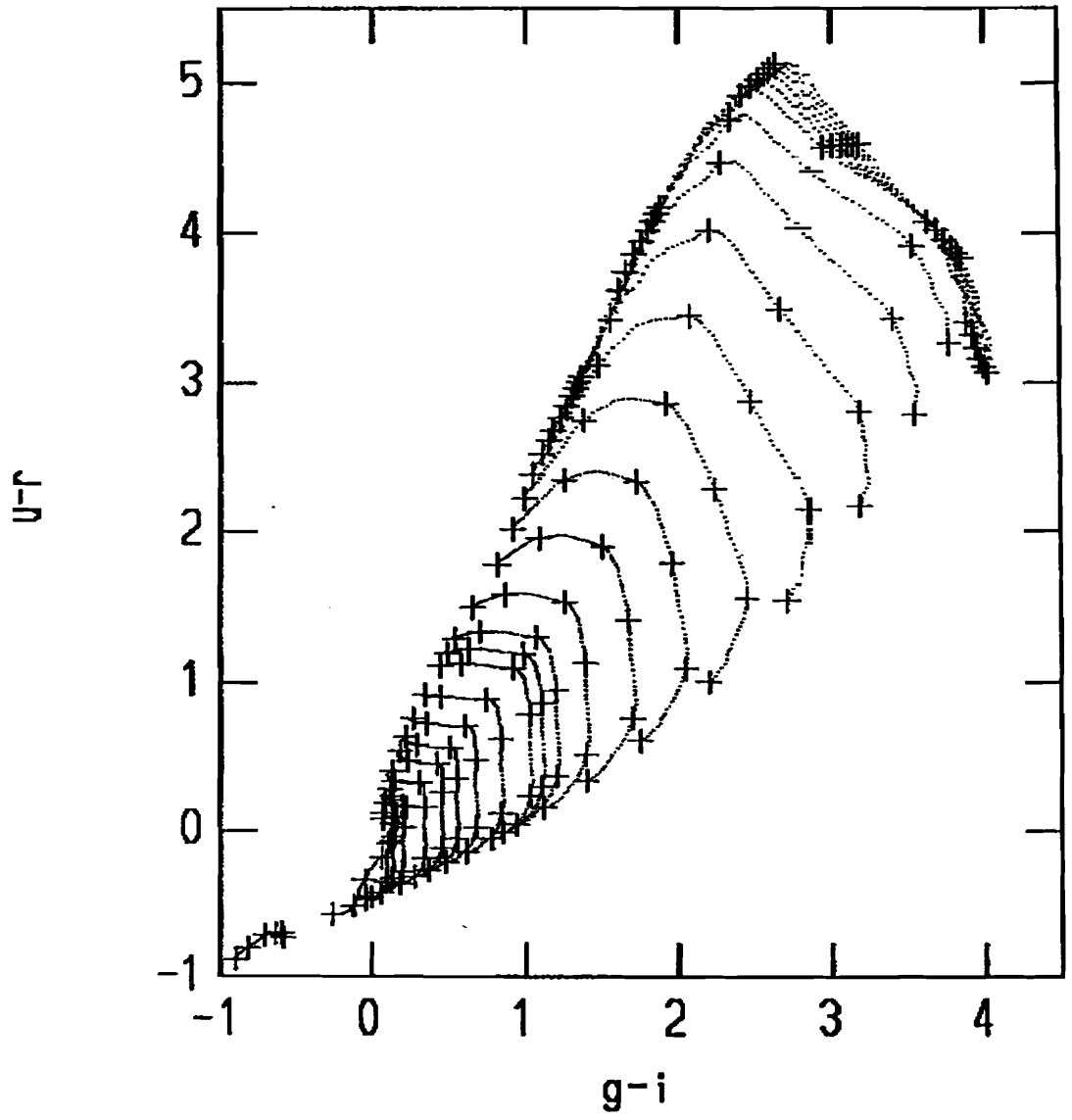

Fig 6

1 A

NOAO/IRAF V2.10EXPORT jtank@oddjob.uchicago.edu Tue 14:44:21 15-Dec-92
colz4g215.ABmag.new
delz<0.2
cross: delz<0.1 point: default

u g r i

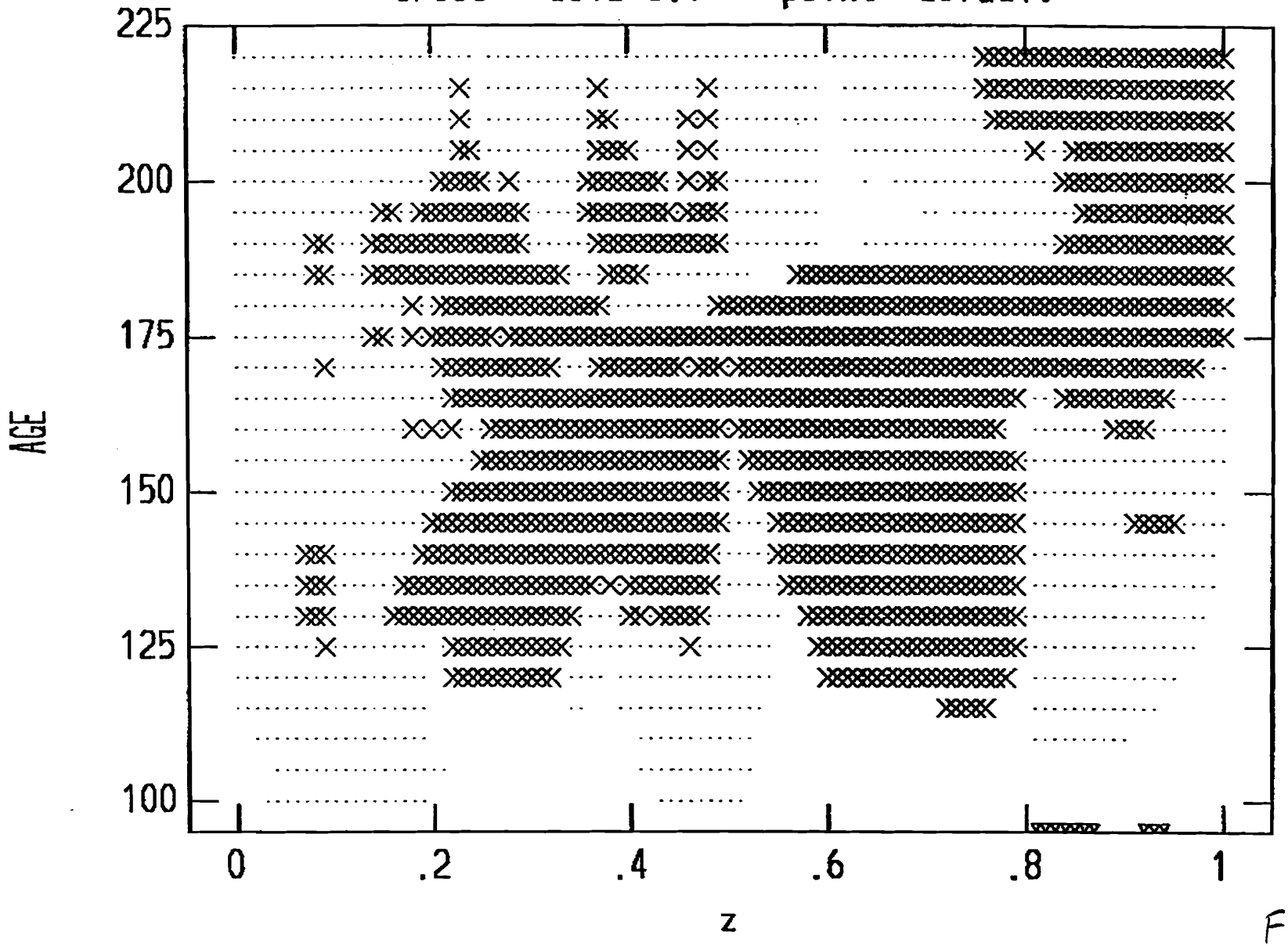

Fig 7

2 A

NOAO/IRAF V2.10EXPORT jtank@oddjob.uchicago.edu Tue 14:42:04 15-Dec-92

colzg215.ABmag.new

ugriz

delz<0.2

cross: delz<0.1 point: default

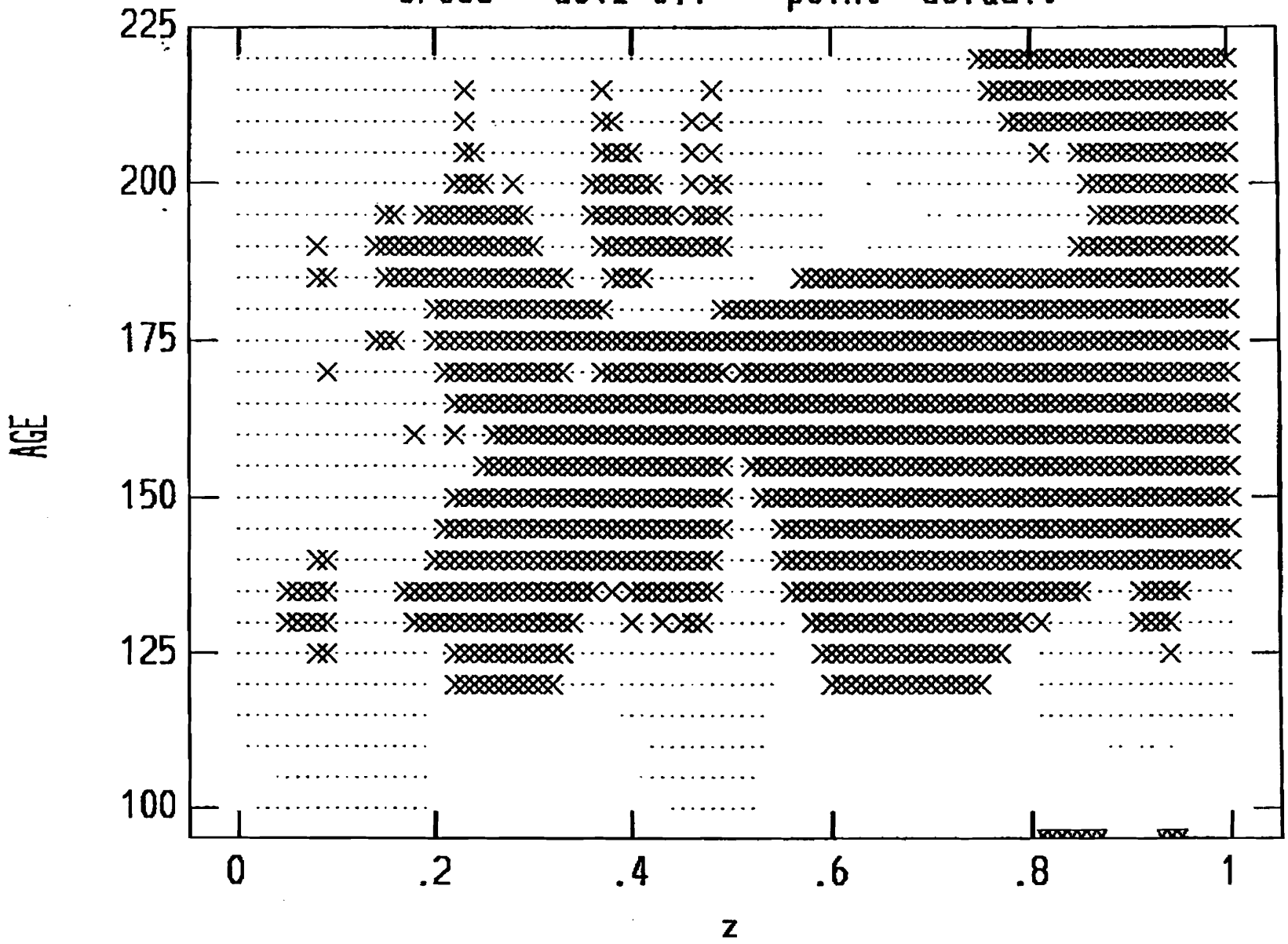

Fig 8

4A

NOAO/IRAF V2.10EXPORT jtank@oddjob.uchicago.edu Tue 13:47:29 15-Dec-92

colz.gstar.g215.ABmag.new

u g* g r i

delz<0.2

~~cross:~~ delz<0.1 point: default

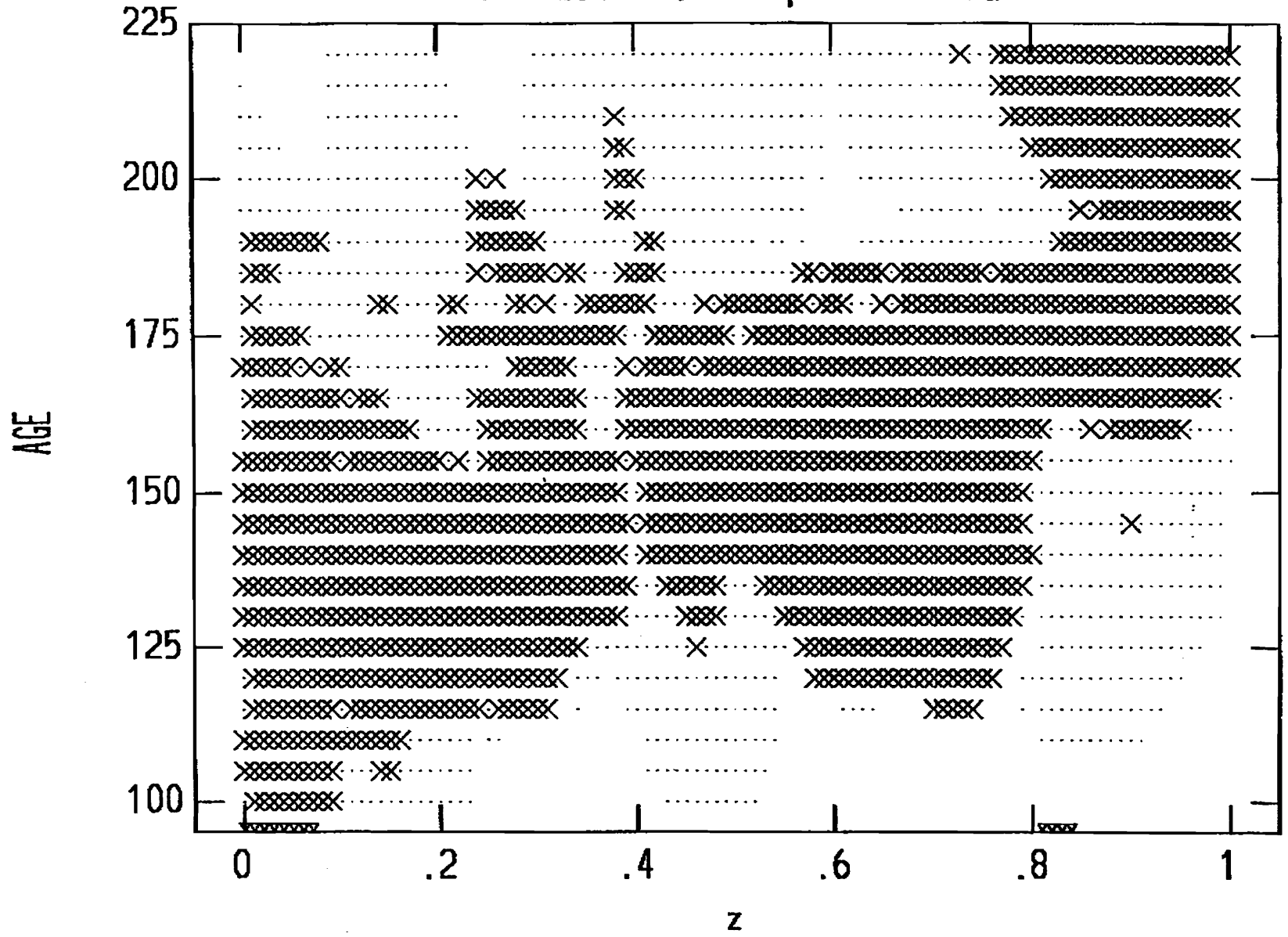

Fig 9

3A

NOAO/IRAF V2.10EXPORT jtank@oddjob.uchicago.edu Tue 14:39:56 15-Dec-92
colz4.2u.g215.ABmag.new
uugri
delz<0.2
cross: delz<0.1 point: default

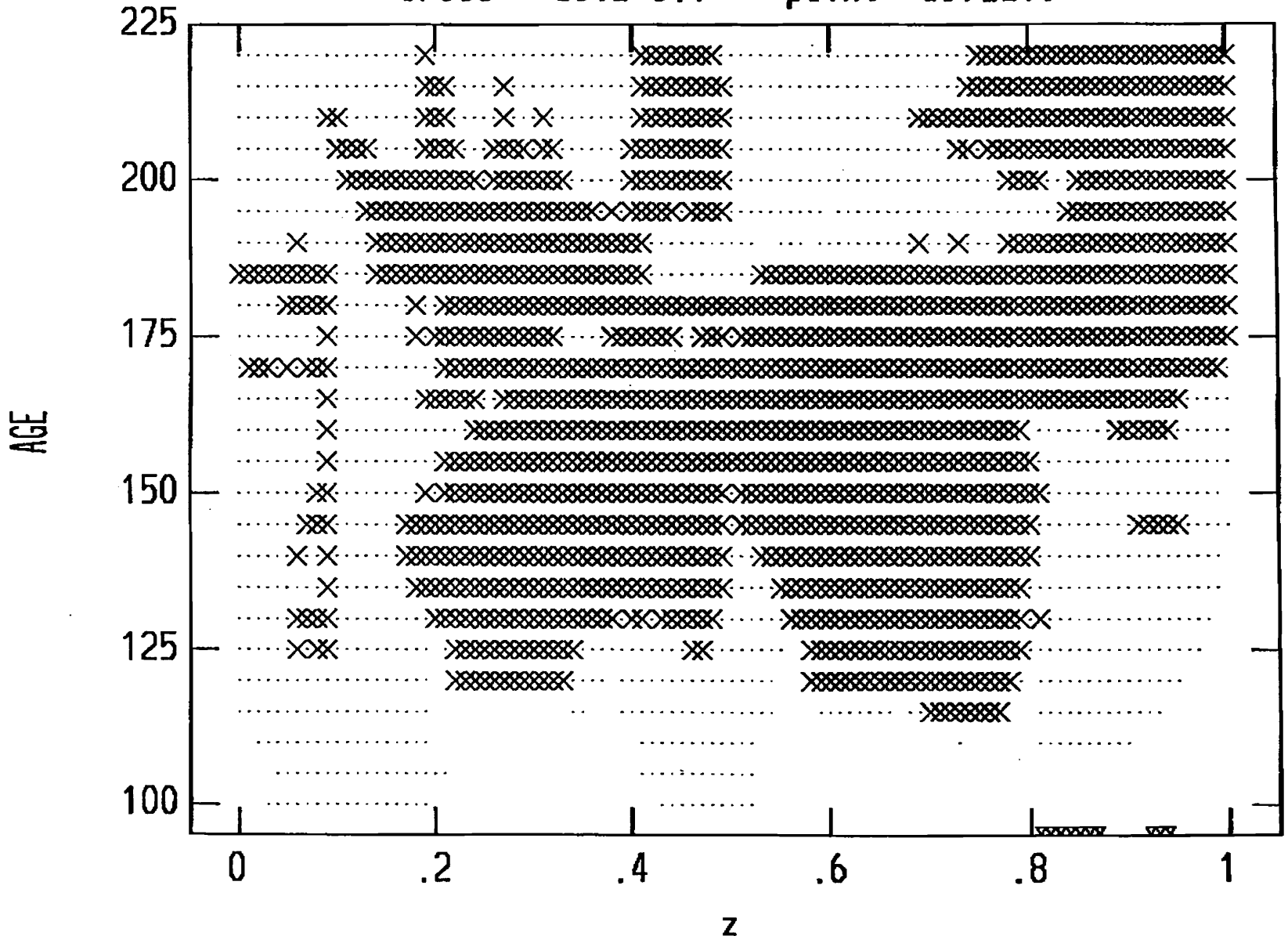

Fig 10

$\alpha = -0.5$

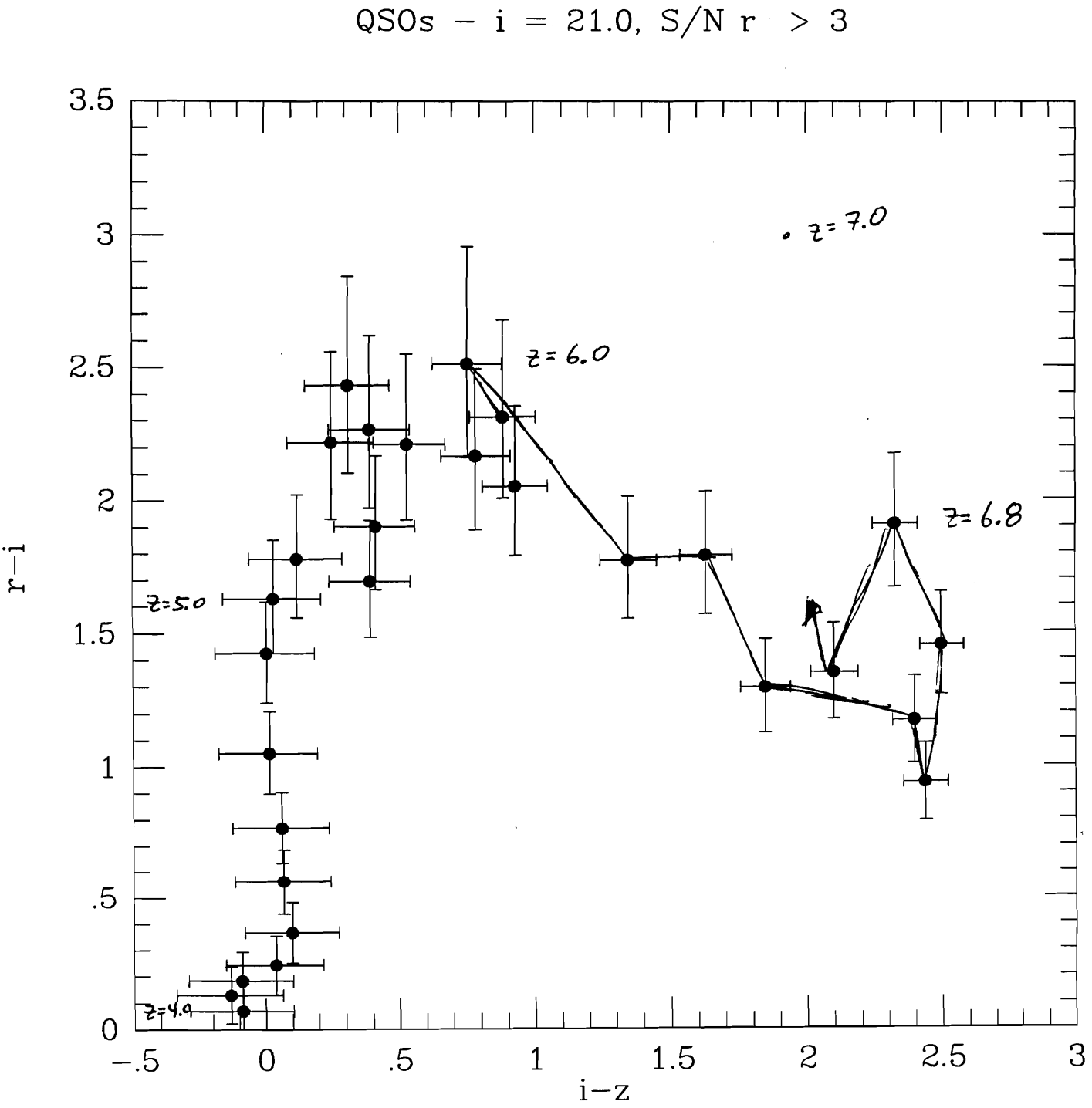

Fig 11

$\alpha = -0.5$

QSOs – $M_{1450} = -26$, S/N r > 3

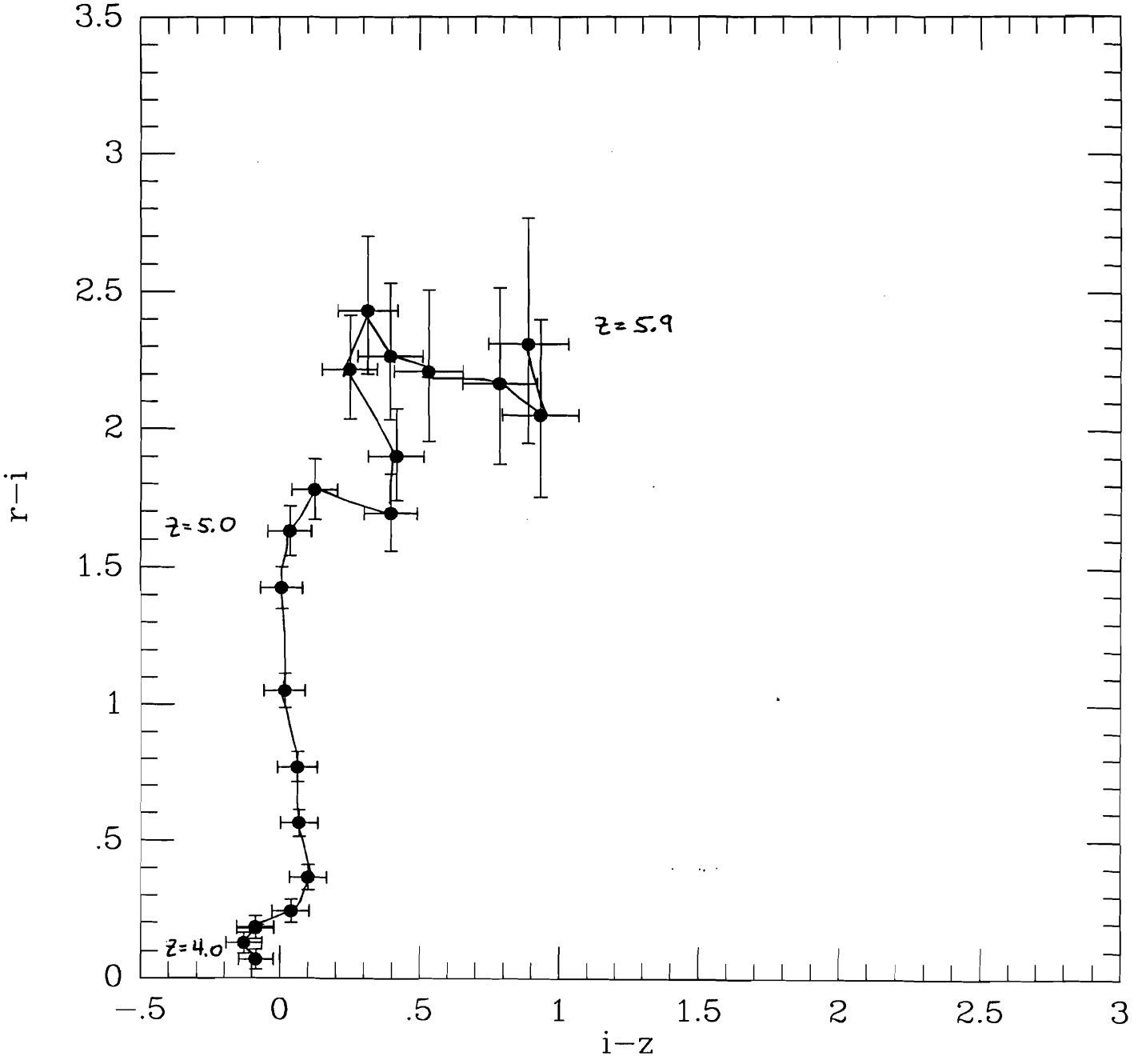

Fig 12

Stars are normalized at i = 21.0

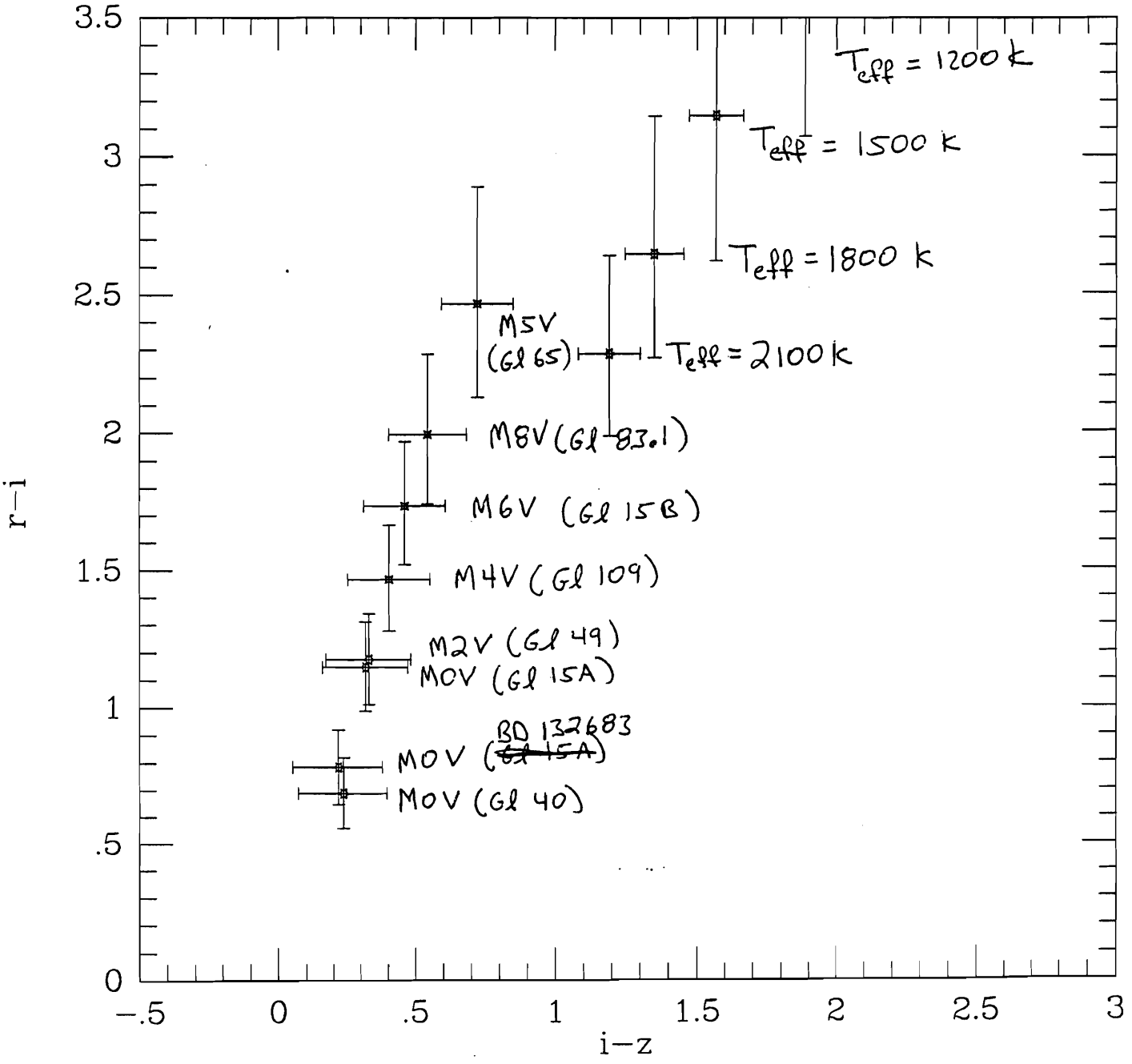

Fig 13

19 December 1992

R.G. Kron Rich

The enclosed report on studies of the SDSS filter complement was distributed to a small group of people for initial reactions before the TOG phone conference on December 17. At that meeting, it was suggested that the report be more widely distributed so that further discussions can progress in the near term. The specific suggestions were:

1) expand the scope of the discussion concerning photometric redshifts for galaxies;

2) change the sensitivity curve of the i band when it is used in conjunction with the z band;

3) explore the degree to which star/quasar separation at all redshifts might be improved by using the u,g*,g,r,i filter combination.

Suggestion 1 is addressed here; the other two suggestions will have to wait until after the holidays, but they should not be difficult to deal with.

The key diagrams are Figures 7,8,9,10. Included here, but not in the first distribution, are the other 12 plots as enumerated below:

Figure 14, 15, 16, 17: g = 22.5, $S/N)_g$ = 12.5, ugri, ugriz, ug*gri, uugri
Figure 18, 19, 20, 21: r = 21.2, $S/N)_r$ = 25.0, ugri, ugriz, ug*gri, uugri
Figure 22, 23, 24, 25: r = 22.0, $S/N)_r$ = 12.5, ugri, ugriz, ug*gri, uugri

The first thing to note is that between g = 21.5 and g = 22.5, and between r = 21.2 and 22.0, there is a very substantial loss of precision in photometric redshifts. This means that the gain in depth over the spectroscopic survey is only about 2.5 magnitudes. Assuming that g = 21.5 is roughly equivalent to B = 21.7, then from Koo & Kron 1992, *ARAA* **30**, 613, there is an empirical determination of what the field galaxy redshift distribution actually is at this depth. Attached as Figure 26 is a model cumulative redshift distribution (which is easier to look at because it is smooth). The median redshift is expected to be about z_{med} = 0.25, and

80% of the galaxies are expected to lie in the interval $0.10 < z < 0.45$ (for a B-selected sample; this makes a difference). On this basis, if our goal is to measure the bulk of the faint-galaxy population with good precision, then this is the redshift range in the plots upon which to concentrate.

The second thing to note is that the various combinations of filters have surprisingly little effect - the differences in the plots are generally subtle. For example, for $g = 21.5$, the plots for ugri and for ugriz (Figures 7 and 8) are essentially the same in the neighborhood of $z = 0.30$. Comparison of these same plots show that adding the z filter does help in the lower right-hand corner, namely the bluer galaxies at $z > 0.8$, which at this magnitude would be expected to be very rare. Figure 9 shows better determination of blue galaxies at low redshift, which is gratifying but possibly not interesting (since for low redshifts $\Delta z/z$ is large).

From the redshift survey with Koo and others, we can plot the "Hess diagram" for a flux-limited sample of faint galaxies, namely the distribution of galaxies in a rest-frame color-magnitude diagram, as shown in Figure 27 (27a gives rest-frame colors, and 27b gives observed-frame colors). Note that the distribution is characterized by a tail to blue colors at low luminosities, and that among the more luminous galaxies, there is a color-luminosity relation that is milder but still significant, especially when seen in the rest-frame. Presumably the sample at $g = 21.5$ will be qualitatively similar, despite the fact that our sample was (mostly) selected in the r band. This translates into an expectation that in a flux-limited sample, the lower-redshift galaxies will tend to be bluer and vice versa. A flipped-around version of Figure 27 can thus serve as an approximate template to the plots of the models to indicate where most of the galaxies may be expected to lie. For those who may wish to pursue this quantitatively, on the next page is a table to convert the "AGE" parameter (called here "# SED") on the plots into a rest-frame color.

Once we have a clear idea of what it is that we want to do with photometric redshifts, then we can decide what part of the galaxy-type — redshift diagram is most important, and then discover which filter system seems to work best there. At that point, we can ask whether the cost of adding *any* fifth filter is really worth the gain, compared to the capabilities of the default ugri, at least as far as galaxy photometric redshifts are concerned.

Zero-redshift colors (AB magnitdes) for varios SEDs sed

# SED	u-g	g-r	r-i	i-z
050	-0.373	-0.505	0.396	-0.215
075	0.077	0.086	0.139	0.063
100	0.201	0.009	0.131	0.070
105	0.230	0.005	0.124	0.067
110	0.277	0.004	0.114	0.062
115	0.378	0.025	0.106	0.055
120	0.466	0.072	0.116	0.058
125	0.540	0.097	0.123	0.064
130	0.637	0.123	0.141	0.078
135	0.756	0.164	0.185	0.104
140	0.884	0.228	0.219	0.120
145	0.935	0.258	0.230	0.122
150	0.993	0.298	0.243	0.124
155	1.114	0.383	0.276	0.131
160	1.288	0.492	0.322	0.144
165	1.446	0.569	0.349	0.153
170	1.591	0.626	0.365	0.158
175	1.714	0.667	0.377	0.162
180	1.814	0.704	0.399	0.172
185	1.884	0.729	0.417	0.179
190	1.931	0.747	0.428	0.184
195	1.993	0.774	0.444	0.190
200	2.047	0.799	0.464	0.199
205	2.093	0.818	0.480	0.204
210	2.132	0.833	0.490	0.208
215	2.163	0.844	0.498	0.211
220	2.190	0.854	0.502	0.213

1B

NOAO/IRAF V2.10EXPORT jtank@oddjob.uchicago.edu Tue 14:44:09 15-Dec-92
colz4g225.ABmag.new
delz<0.2
cross: delz<0.1 point: default

g = 22.5
S/N)$_g$ = 12.5

ugri

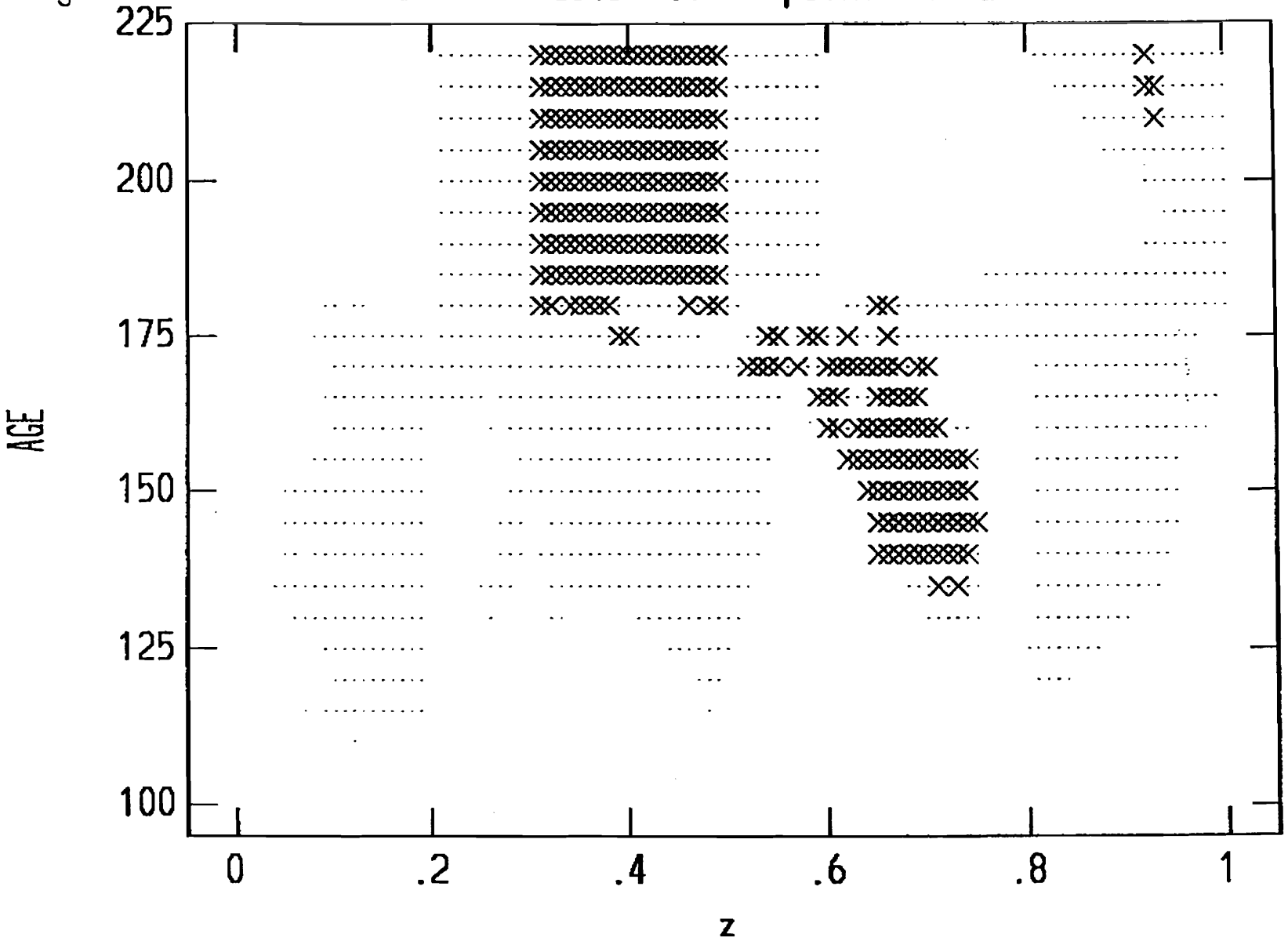

Fig 14

2B

NOAO/IRAF V2.10EXPORT jtank@oddjob.uchicago.edu Tue 14:42:17 15-Dec-92

colzg225.ABmag.new

u g r i z

delz<0.2

~~cross:~~ delz<0.1 point: default

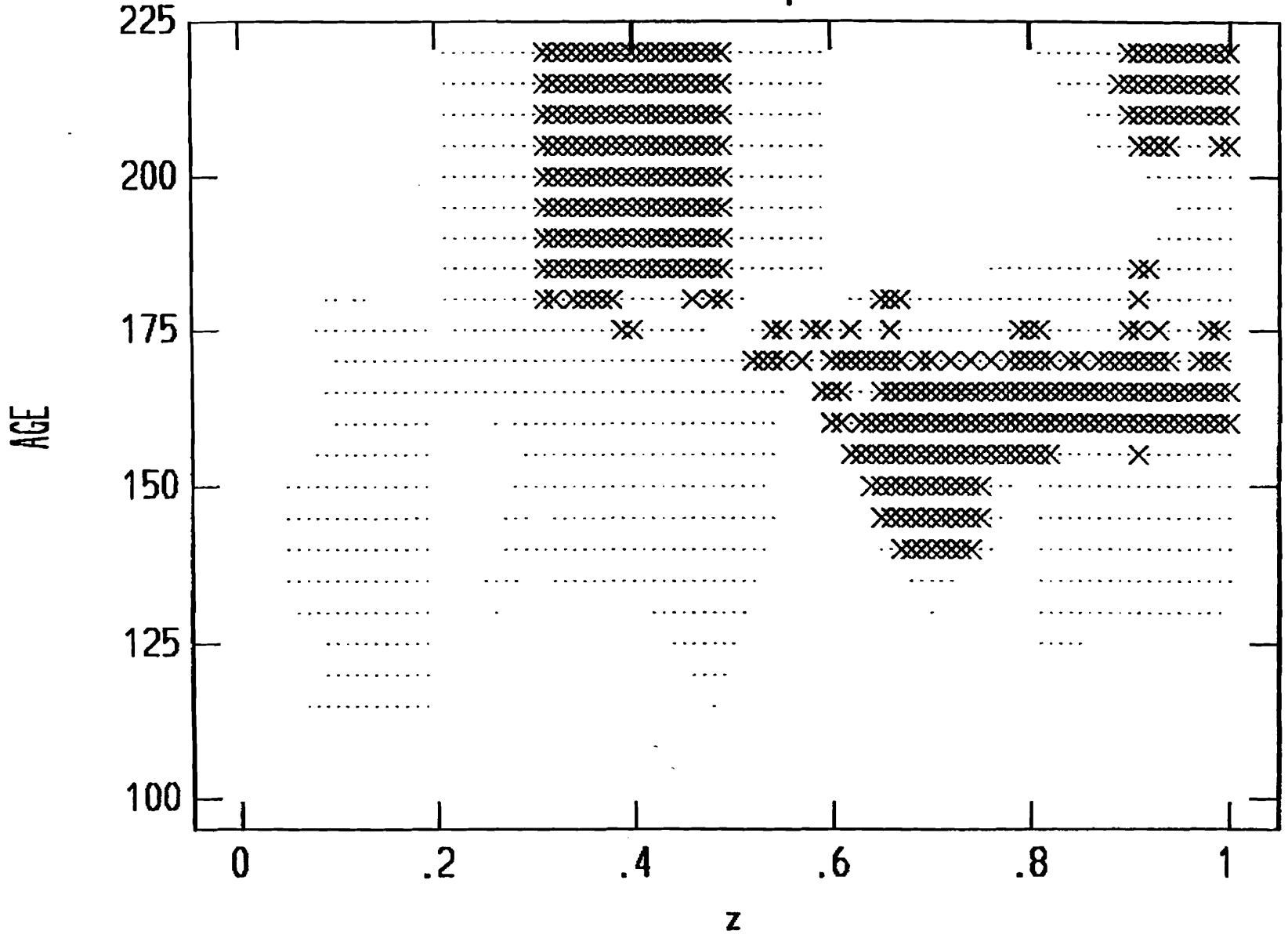

Fig 15

4B

NOAO/IRAF V2.10EXPORT jtank@oddjob.uchicago.edu Tue 13:47:45 15-Dec-92
colz.gstar.g225.ABmag.new
u g* g ri
delz<0.2
cross: delz<0.1 point: default

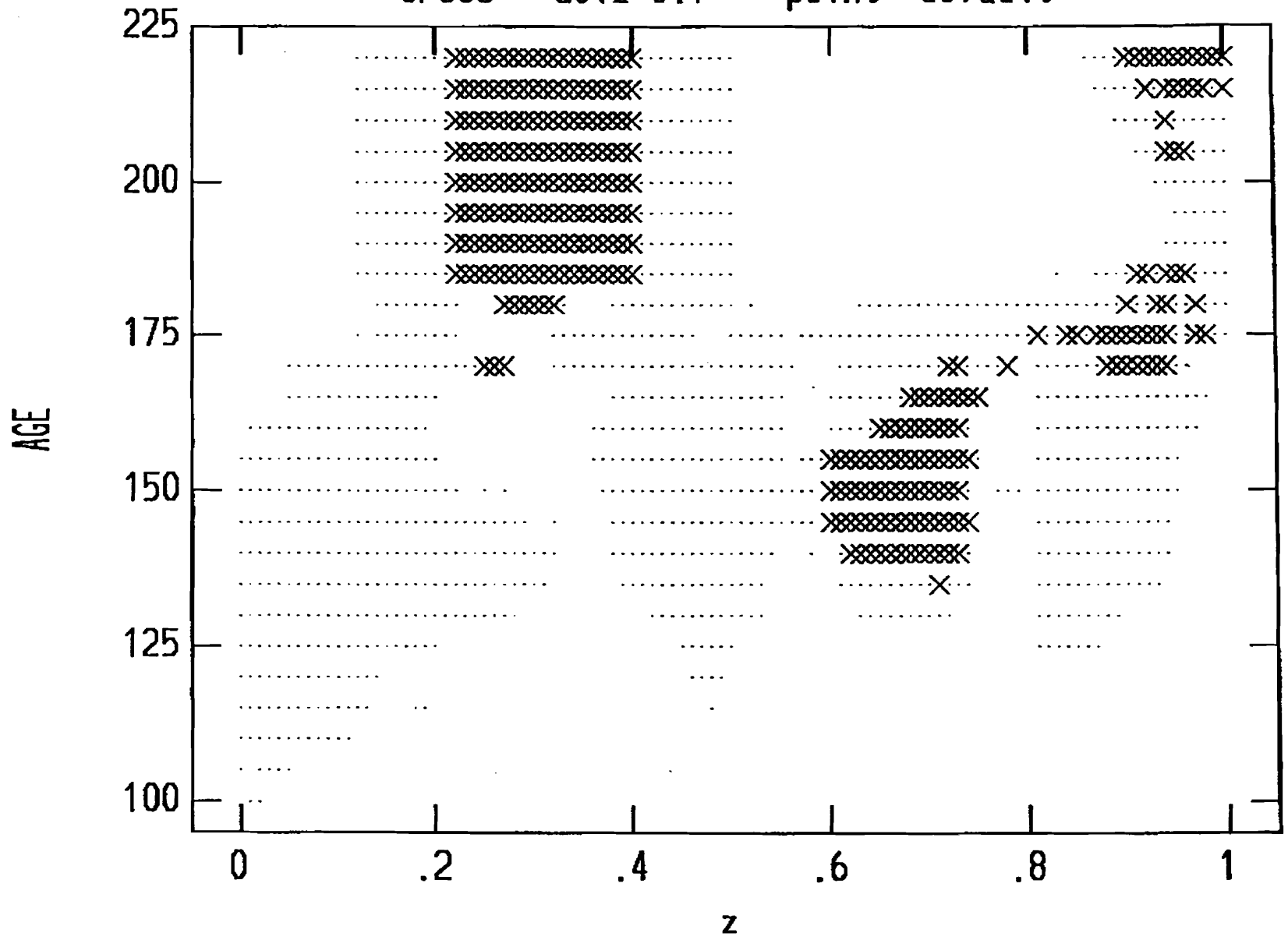

Fig 16

3B

NOAO/IRAF V2.10EXPORT jtank@oddjob.uchicago.edu Tue 14:40:14 15-Dec-92

colz4.2u.g225.ABmag.out

u u g r i

delz<0.2

cross: delz<0.1 point: default

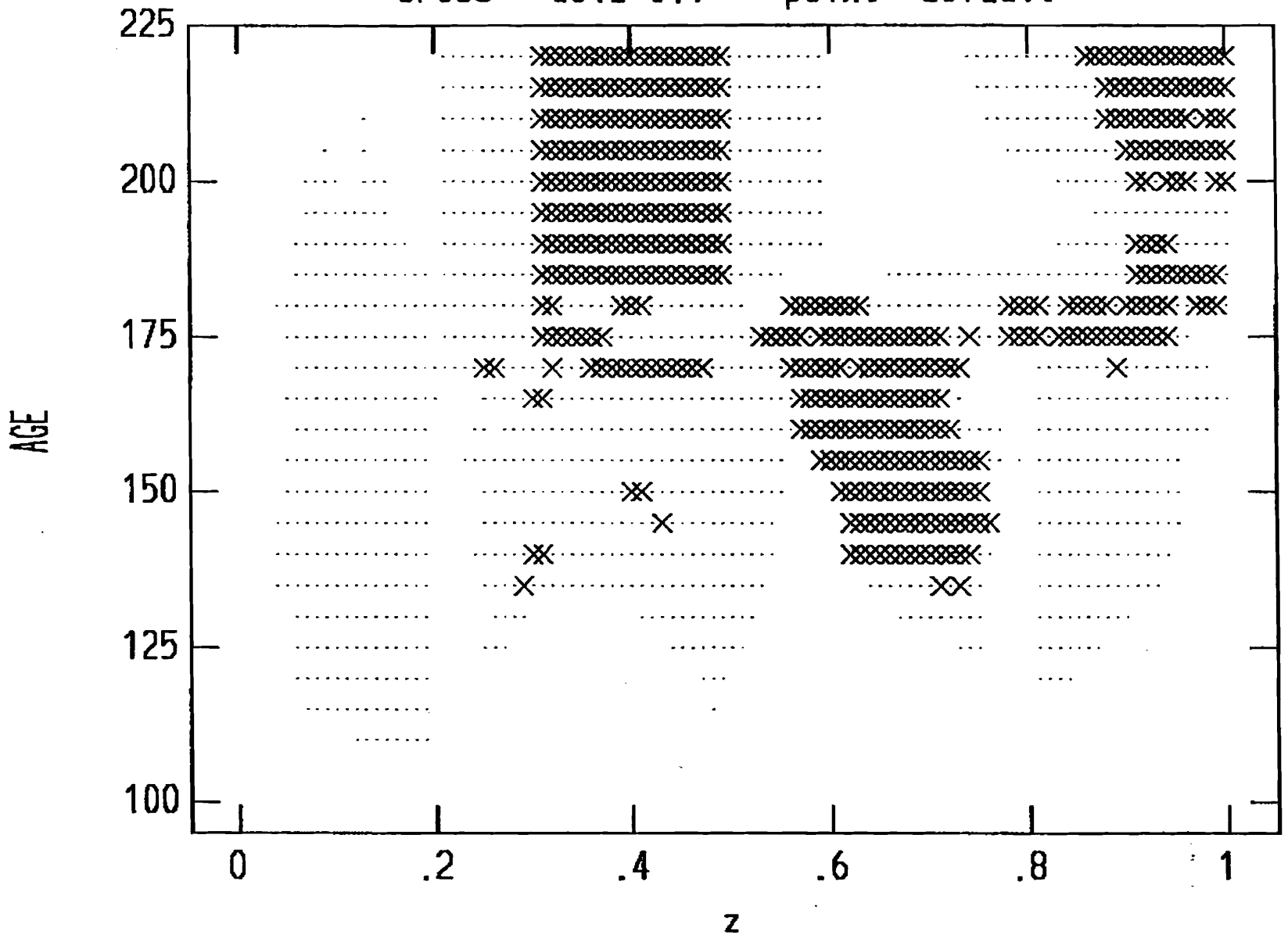

Fig 17

1 C

NOAO/IRAF V2.10EXPORT jtank@oddjob.uchicago.edu Tue 14:44:35 15-Dec-92

colz4r212.ABmag.new

delz<0.2

cross: delz<0.1 point: default

r = 21.2

S/N)$_r$ = 25

ugri

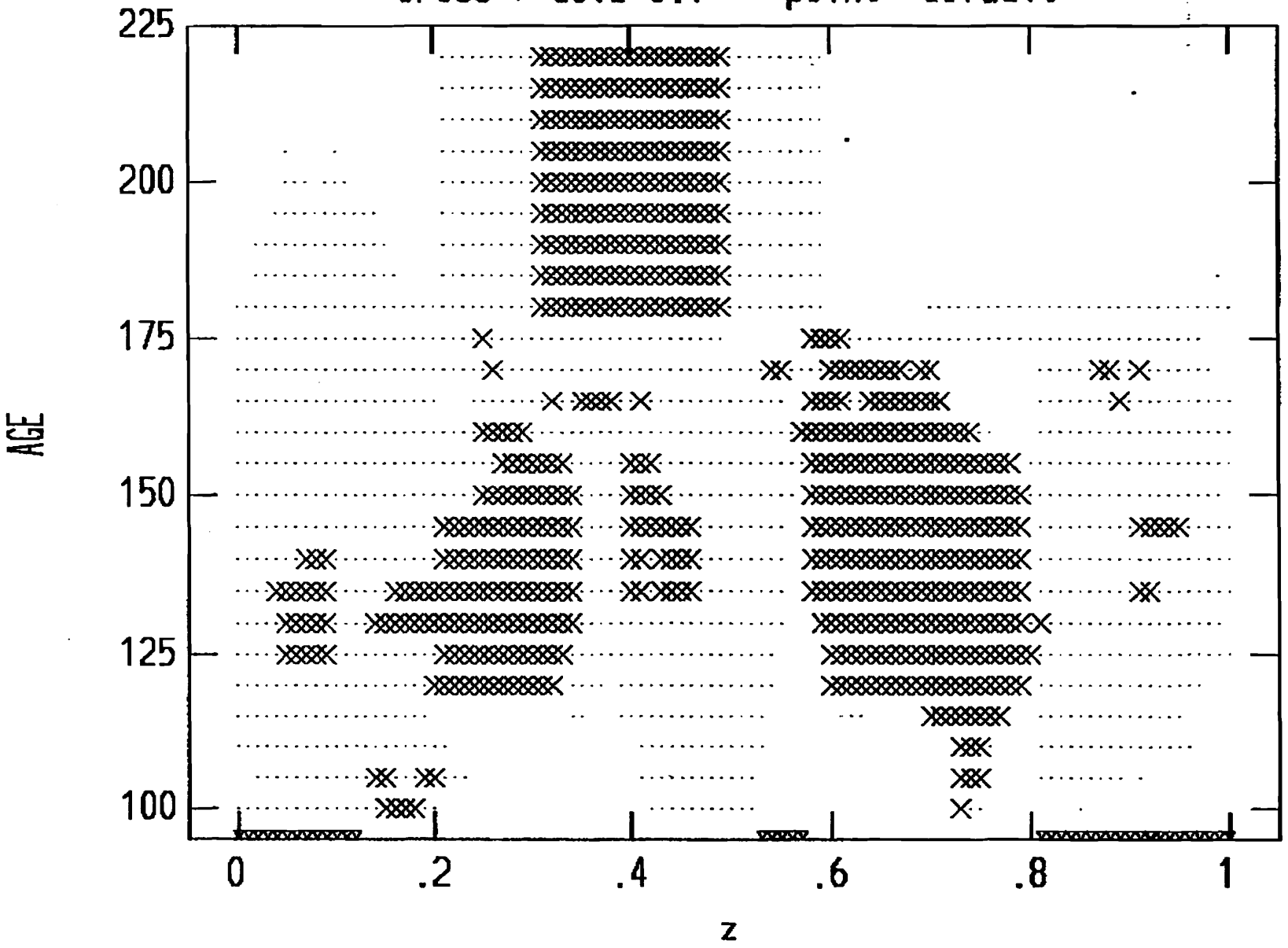

Fig 18

2C

NOAO/IRAF V2.10EXPORT jtank@oddjob.uchicago.edu Tue 14:42:31 15-Dec-92

colzr212.ABmag.new

u g r i z

delz<0.2

cross: delz<0.1 point: default

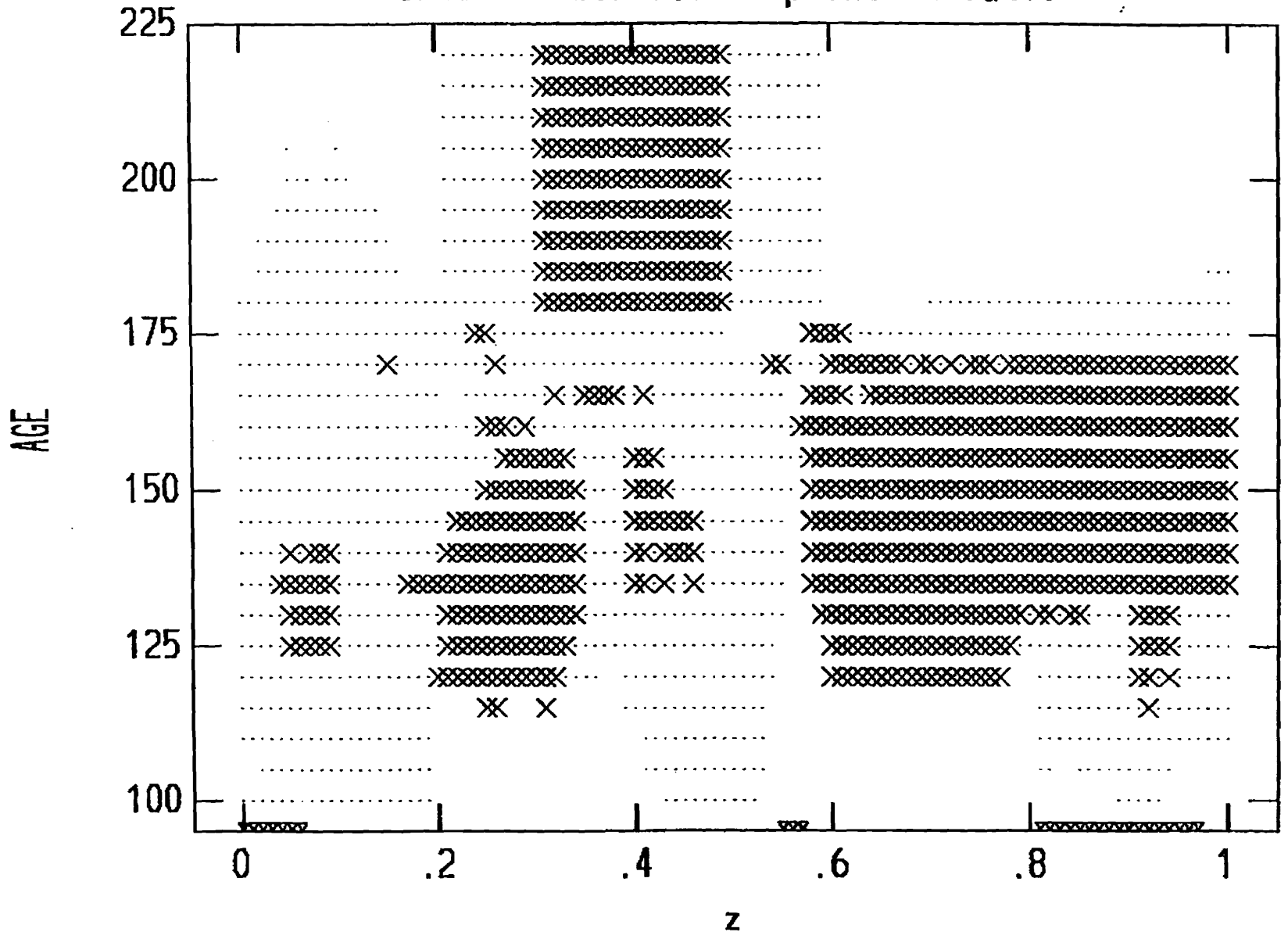

Fig 19

4C

NOAO/IRAF V2.10EXPORT jtank@oddjob.uchicago.edu Tue 13:48:03 15-Dec-92

colz.gstar.r212.ABmag.out

u g* g r i

delz<0.2

cross: delz<0.1 point: default

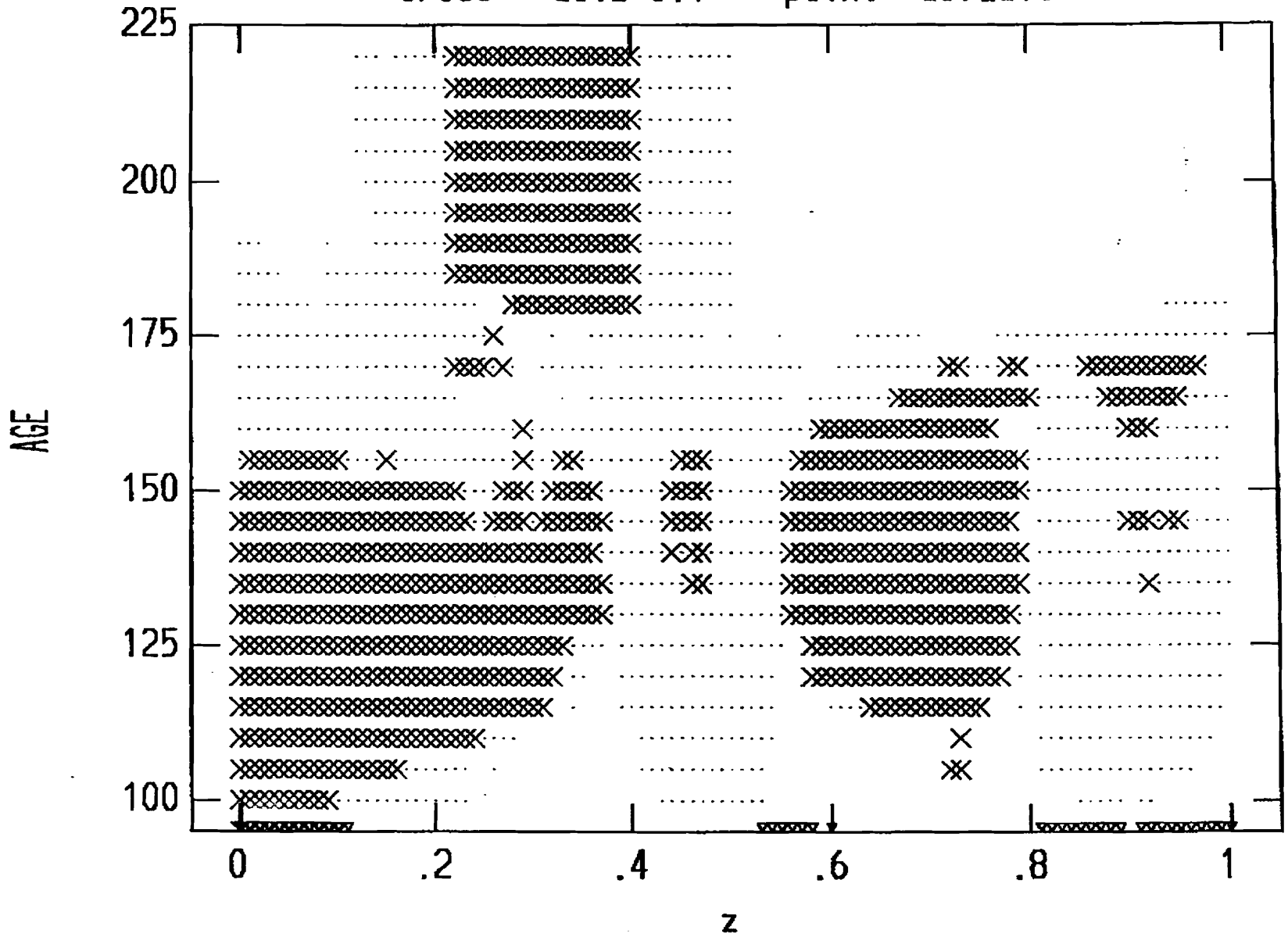

Fig 20

3C

NOAO/IRAF V2.10EXPORT jtank@oddjob.uchicago.edu Tue 14:40:28 15-Dec-92
colz4.2u.r212.ABmag.out
u u g r i
delz<0.2
cross: delz<0.1 point: default

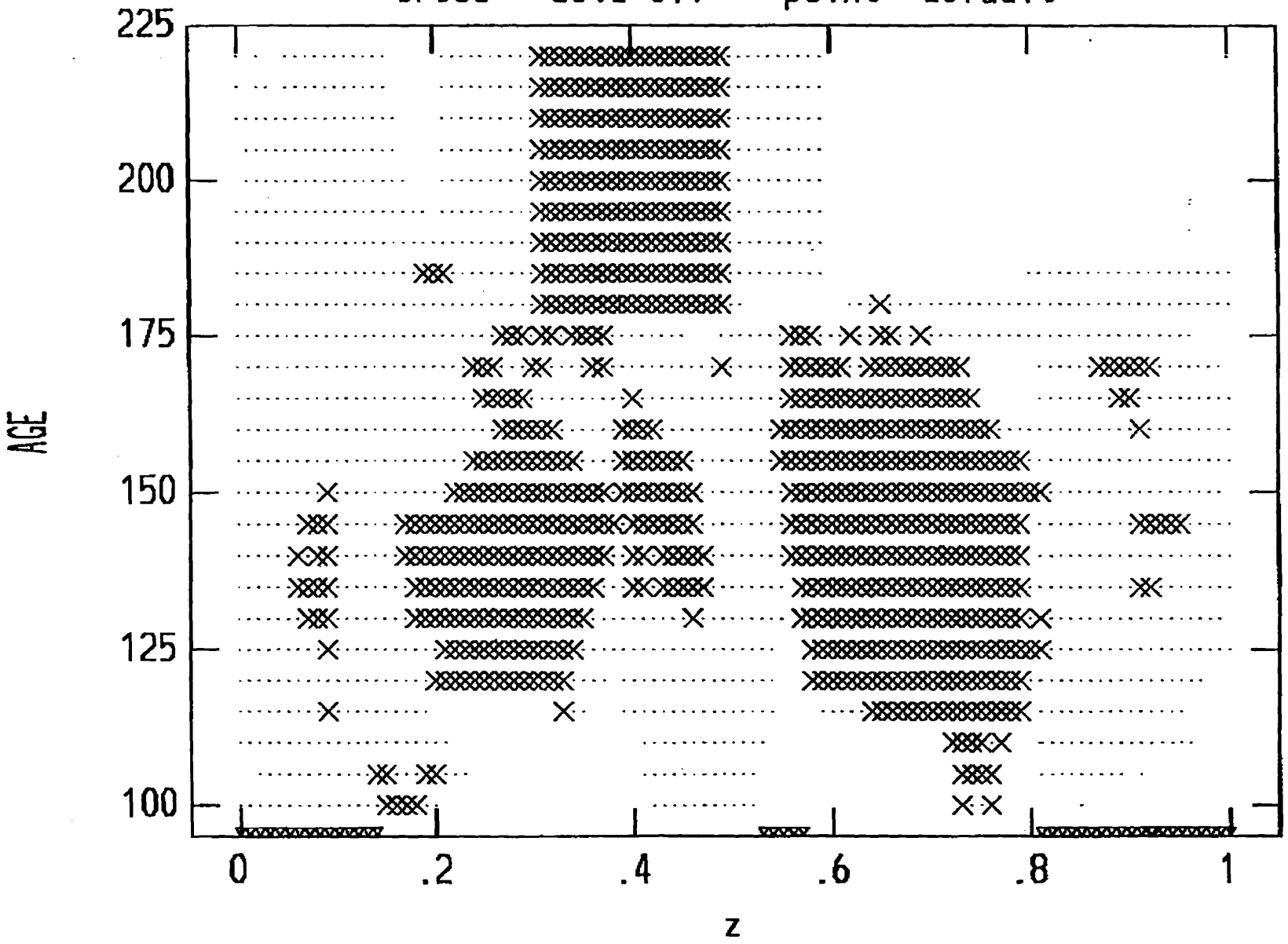

Fig 21

NOAO/IRAF V2.10EXPORT jtank@oddjob.uchicago.edu Tue 14:44:46 15-Dec-92

colz4r22.ABmag.new

delz<0.2

cross: delz<0.1 point: default

r = 22.0

$(S/N)_r = 12.5$

u g r i

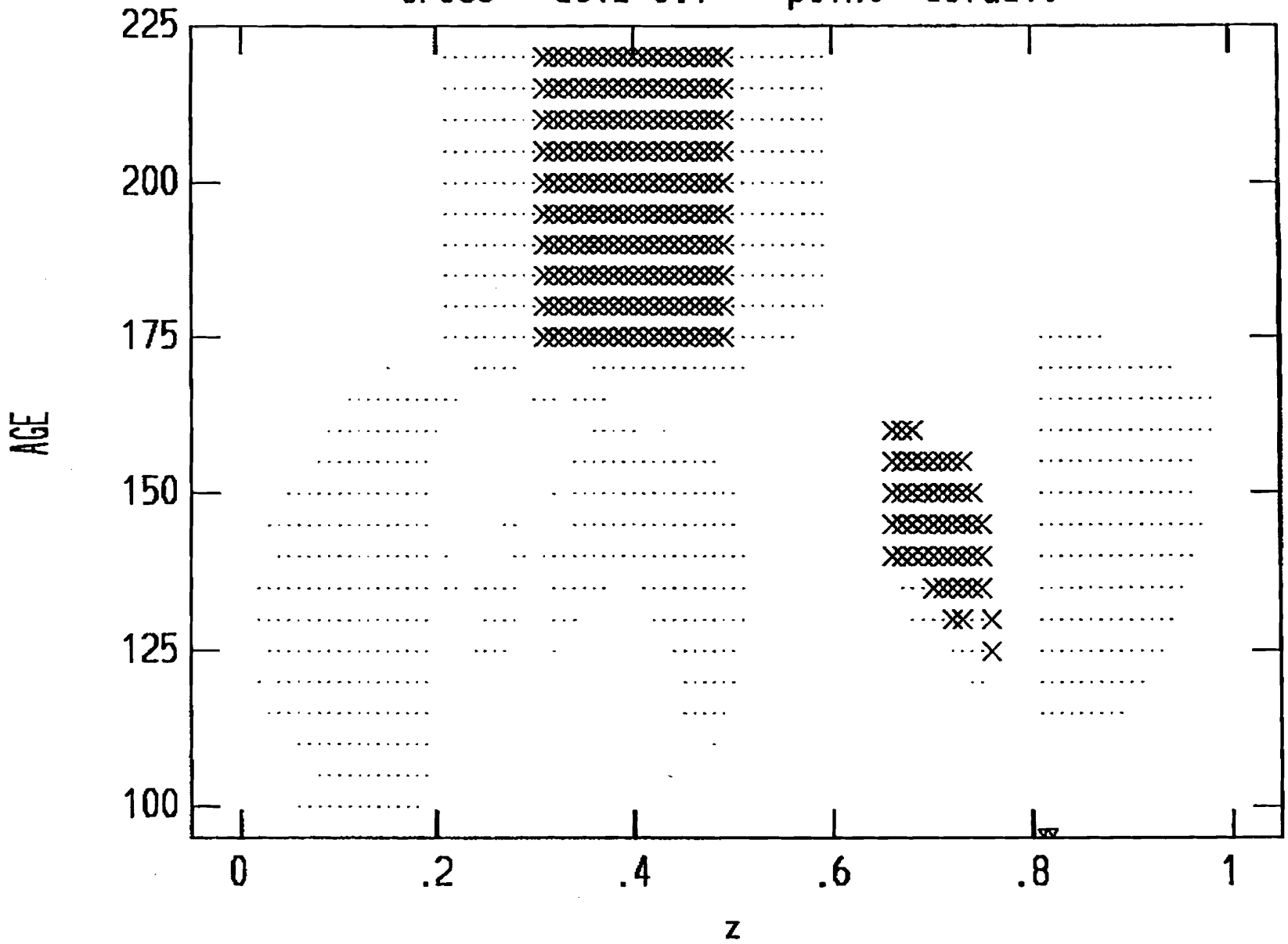

Fig 22

2D

NOAO/IRAF V2.10EXPORT jtank@oddjob.uchicago.edu Tue 14:42:42 15-Dec-92

colzr22.ABmag.new

u s r i z

delz<0.2

cross: delz<0.1 point: default

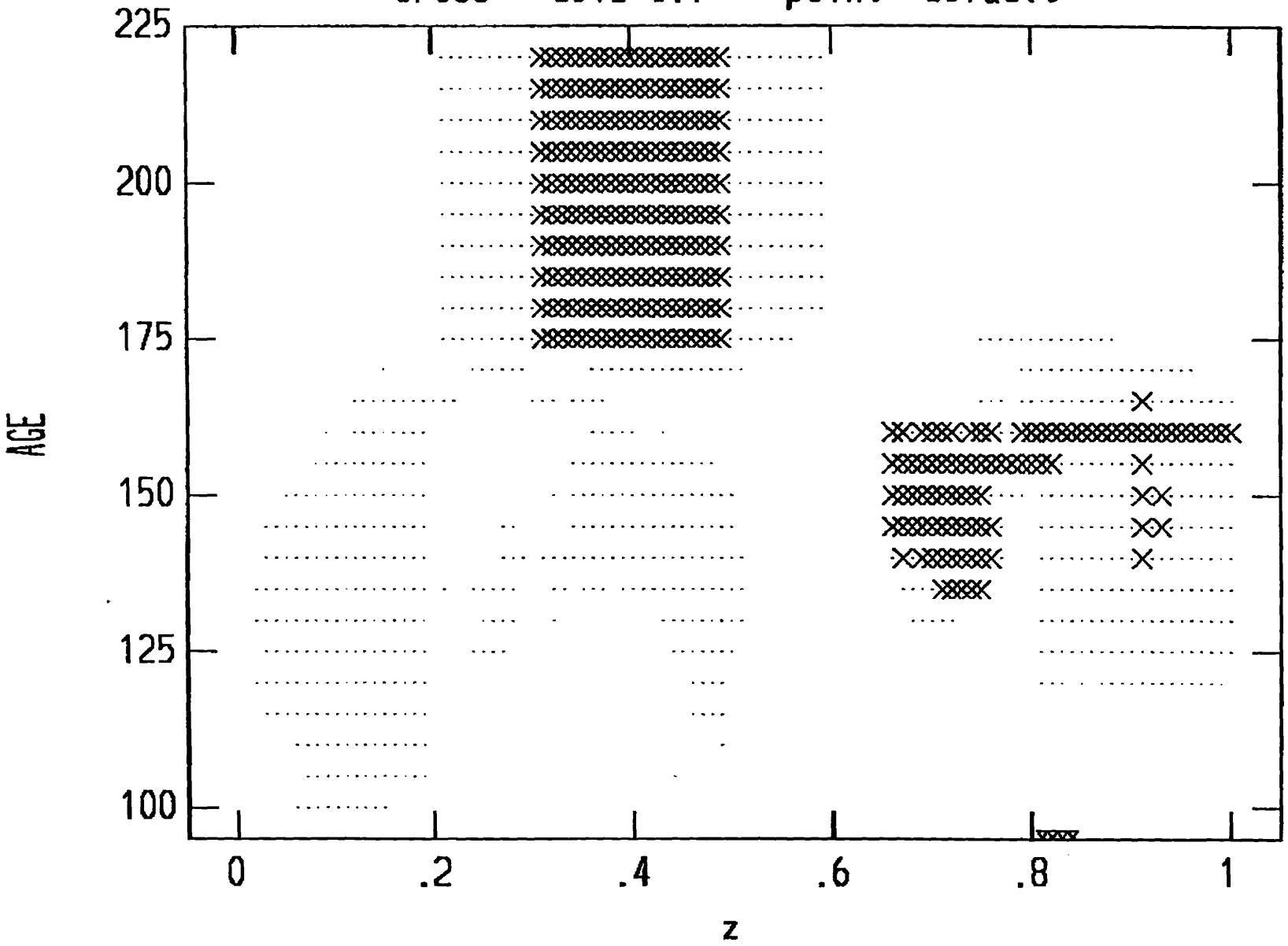

Fig 23

40

NOAO/IRAF V2.10EXPORT jtank@oddjob.uchicago.edu Tue 13:49:06 15-Dec-92

colz.gstar.r22.ABmag.new

u g* g r i

delz<0.2

cross: delz<0.1 point: default

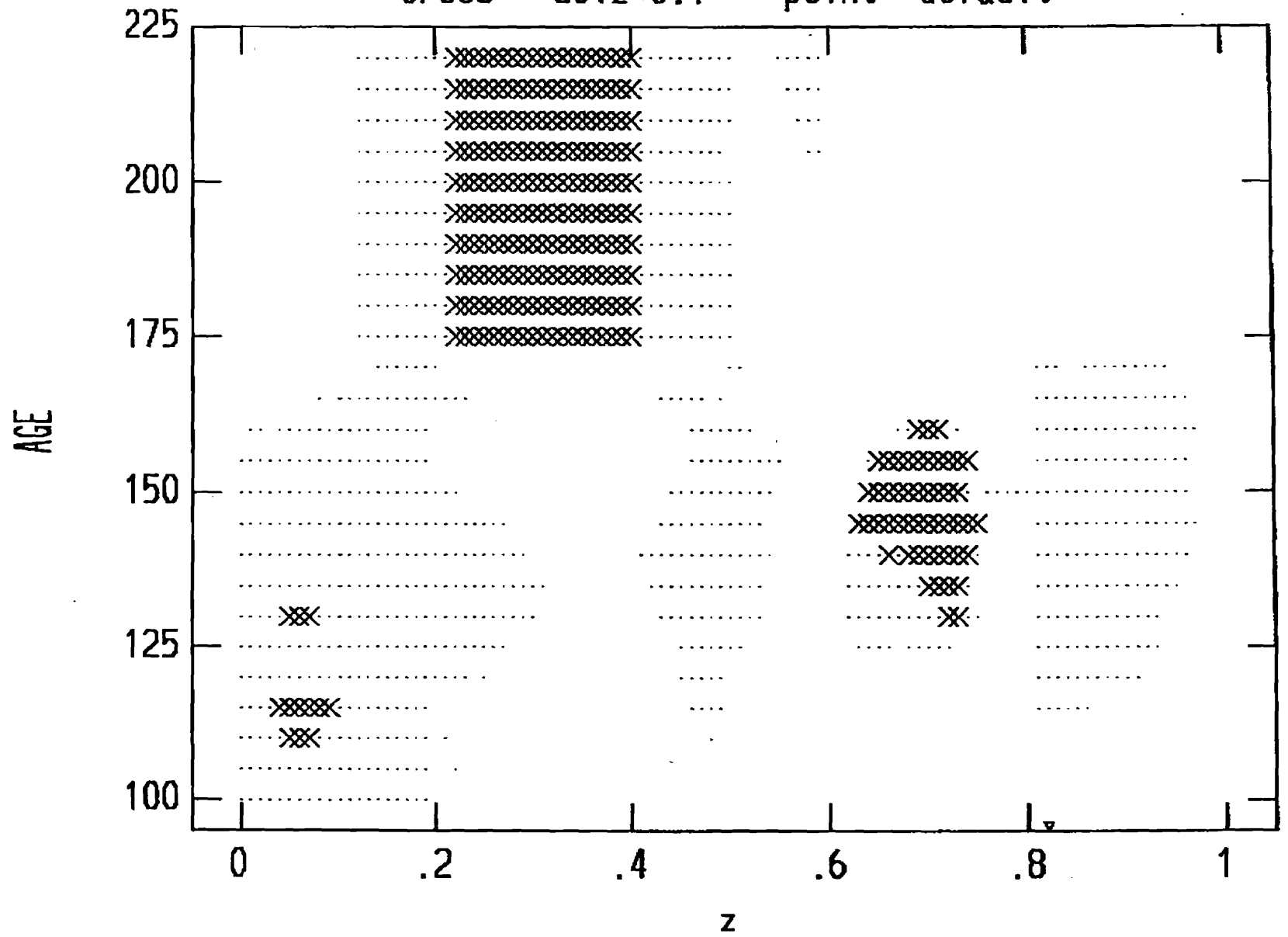

Fig. 24

30

NOAO/IRAF V2.10KPORT jtank@oddjob.uchicago.edu Tue 14:40:39 15-Dec-92
colz4.2u.r22.ABmag.out
u u g r i
delz<0.2
cross: delz<0.1 point: default

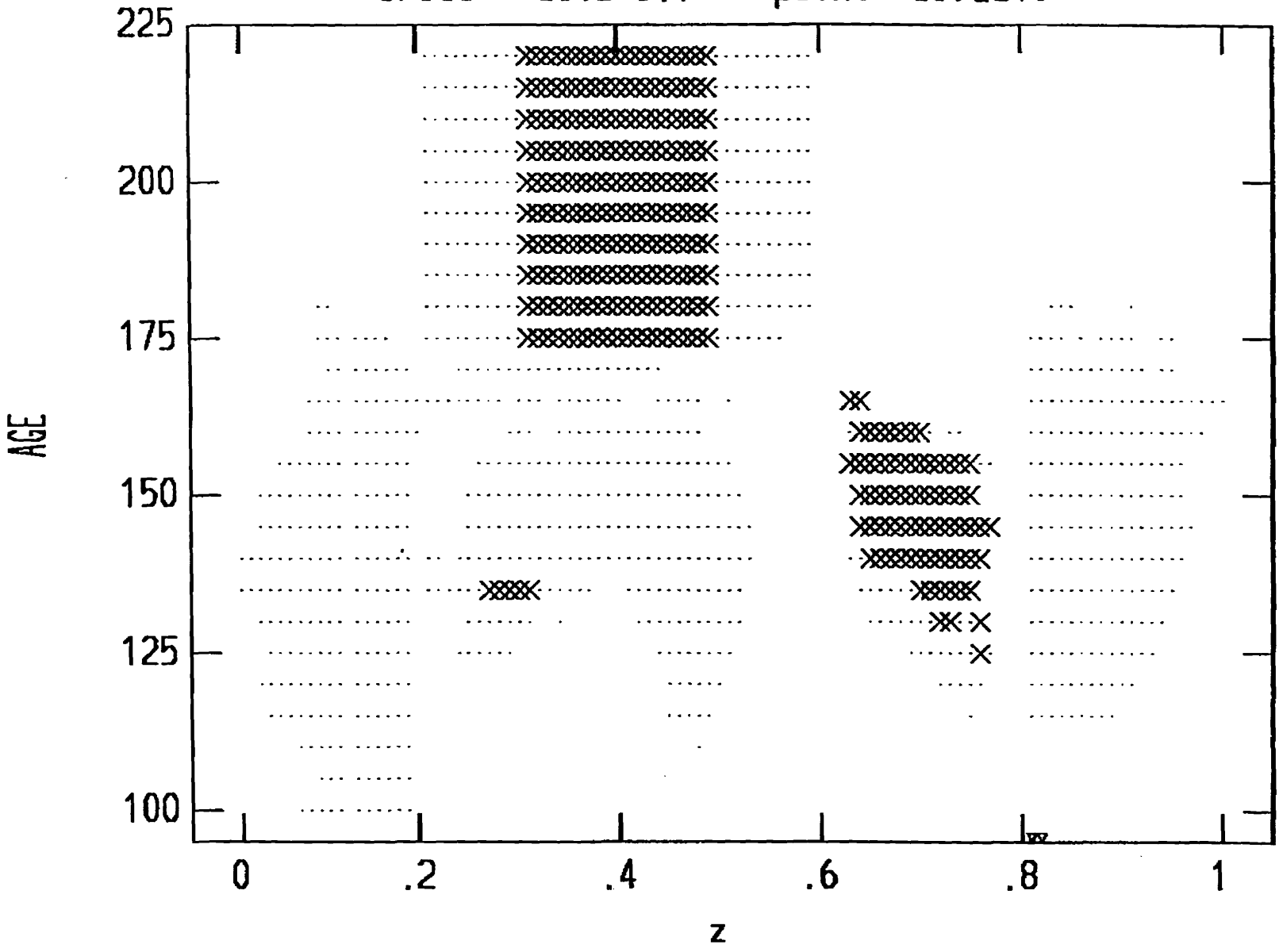

Fig 25

CHICAGO ASTRO-PHYSICS

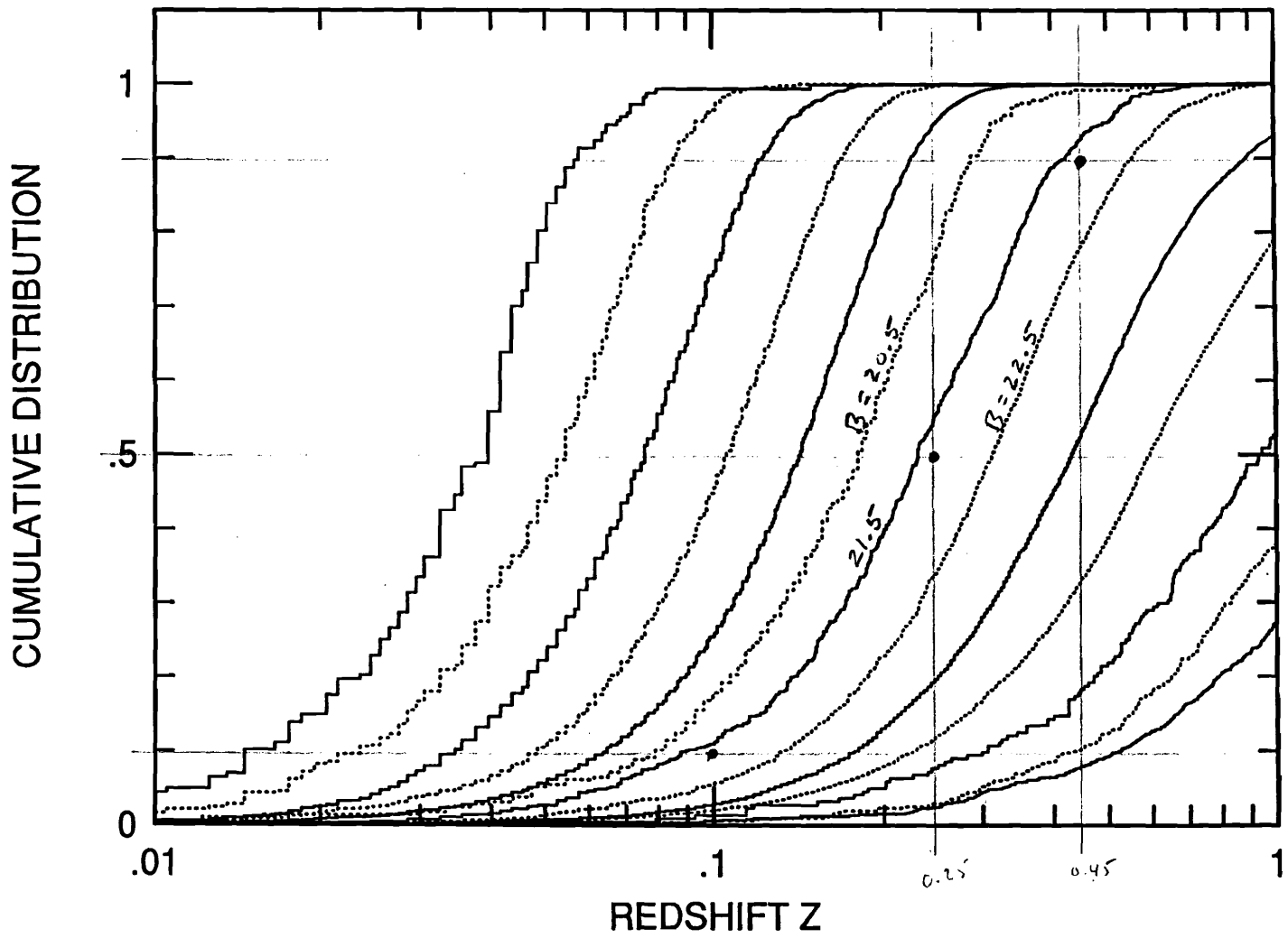
CUMULATIVE DISTRIBUTION
1
.5
0
.01
.1
1
REDSHIFT Z
0.25
0.45
β=20.5
21.5
β=22.5

Fig 26

Galaxies in SA57 and SA68

Fig 27a

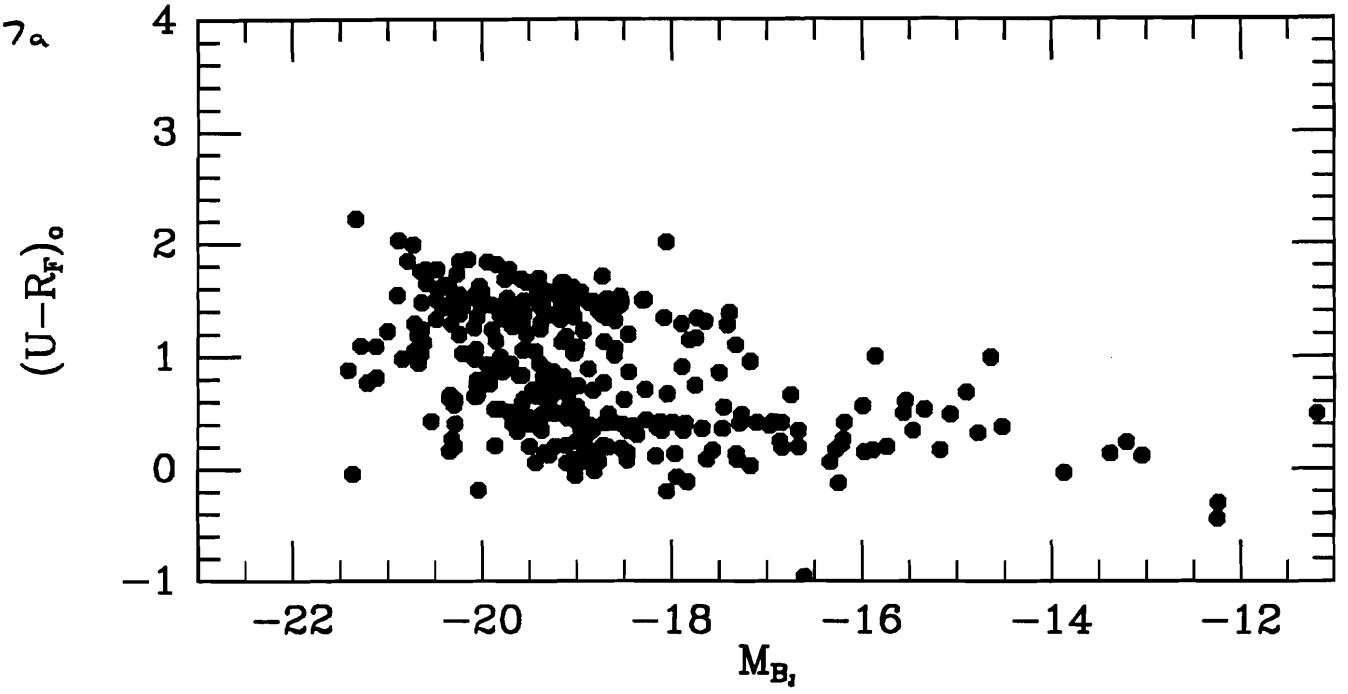
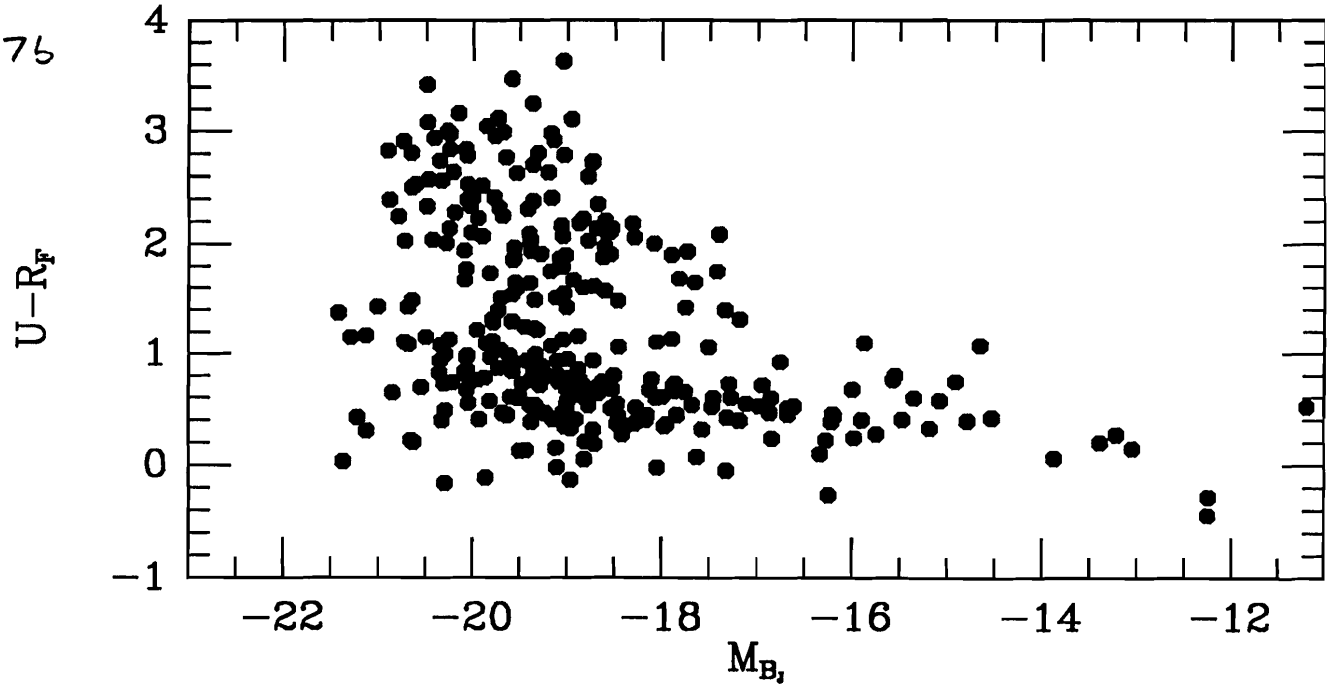
Fig 27b